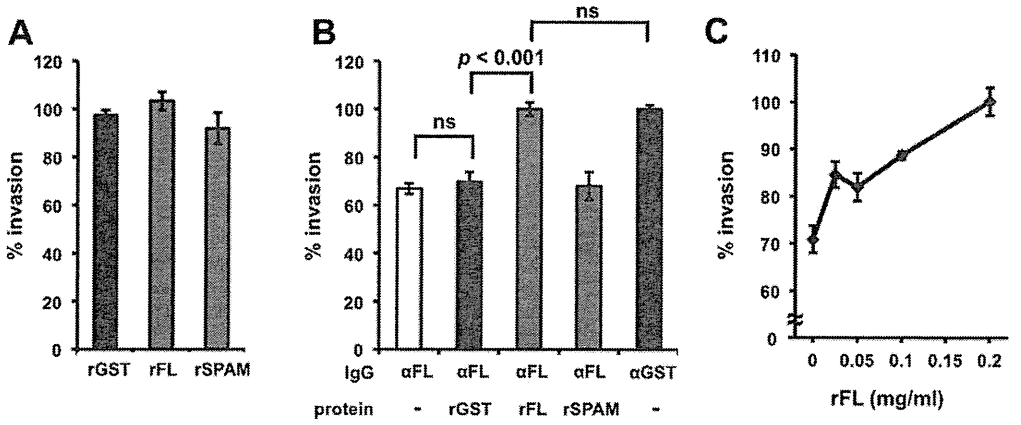

Fig. 5. The inhibitory activity of anti-PfMSPDBL1 antibodies is neutralized by the rFL protein, but not rSPAM. (A) Recombinant proteins used for the neutralization did not inhibit parasite invasion. Percent invasion of the parasites for 3D7 strain in the presence of 0.2 mg/ml of each recombinant protein were measured. Statistical analysis was performed using One-way ANOVA and there was no significant difference. (B) The invasion inhibition with the anti-rFL IgG was neutralized by the addition of rFL protein. Percent invasion for the 3D7 strain were determined in the presence of 20 mg/ml of anti-rFL IgG and 0.2 mg/ml of each recombinant protein. Anti-rFL and -GST IgGs (without any recombinant proteins) (–) were used as a positive and a negative control, respectively. Statistical analysis was performed using One-way ANOVA followed by Bonferroni's pairwise multiple comparison tests. (C) Percent invasion of the 3D7 wild type strain in the presence of 20 mg/ml of anti-rFL IgG and rFL protein at increasing concentrations. For all panels, the error bars represent standard error of the mean (SEM) of three independent experiments. For panel B and C, anti-rFL IgG was pre-incubated with recombinant proteins for 1 h and then tested for inhibition.

compare each experimental group to the control. To compare both total percentage growth and ratio of different stages (i.e., trophozoite, early schizont, and late schizont) separately among the three groups in the growth inhibition assay (Fig. 4C) a one-way ANOVA test was performed. To compare the parasitemia in the GIAs using 3D7 wild type and 3D7ΔDBL1 parasites (Fig. 4D), a *F*-test was performed to compare variances, followed by a Student's *t*-test. For an ELISA using human sera (Fig. 6), the antibody responses were not normally distributed and therefore a Mann–Whitney *U*-test was performed comparing medians of the OD values. All statistical analyses were calculated by GraphPad Prism software (GraphPad Software, San Diego, CA).

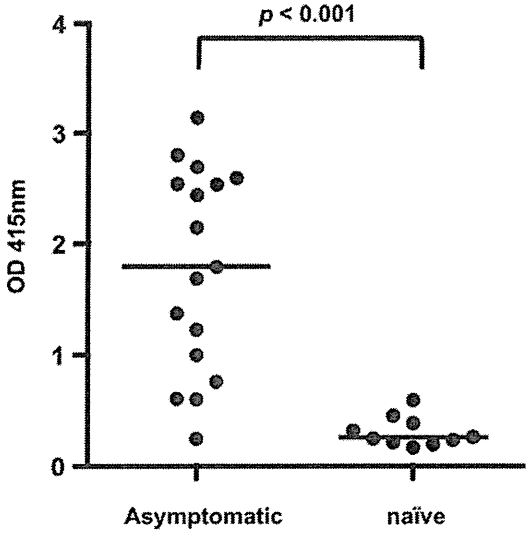

Fig. 6. Antibodies to PfMSPDBL1 are elicited in human sera in malaria-endemic area. Antibody responses to rFL in human serum samples were measured with ELISA. The serum samples were obtained from asymptomatic ($n = 17$) or malaria naïve ($n = 10$) adult individuals from malaria-endemic area in Thailand. Two independent assays were performed, and in each assay samples were analyzed in duplicate. Each dot represents the mean of two assays and the bars represent median of each dot. Statistical analysis was performed using the Mann–Whitney *U*-test to compare the medians.

3. Results

3.1. Synthesis of recombinant PfMSPDBL1 proteins using a wheat germ cell-free system

We designed two recombinant proteins, i.e., rFL and rSPAM of PfMSPDBL1 (Fig. 1A) and expressed them using the wheat germ cell-free system. Fig. 1C shows the recombinant proteins resolved in a 12.5% SDS-polyacrylamide gel. Almost all of the recombinant PfMSPDBL1 proteins were recovered in the soluble fraction and easily purified as a single dominant band (Fig. 1C, arrows) by affinity chromatography. The yields of purified rFL and rSPAM proteins were 73 and 62 μg/6.0 ml of the reaction mixture, respectively. These results demonstrate that the wheat germ cell-free system is able to express PfMSPDBL1 as a soluble protein.

3.2. Anti-PfMSPDBL1 antibodies are specific for native PfMSPDBL1

In order to characterize the PfMSPDBL1 protein, a rabbit was immunized with rFL protein. The reactivity of anti-rFL serum was evaluated using schizont-rich parasites by Western blot analysis. To confirm the specificity of the antiserum, lysates of schizont from 3D7 (WT) and the 3D7ΔDBL1 (KO) (Uboldi et al., in preparation) parasites were analyzed (Fig. 2A). Comparison of the reactivity between WT and KO demonstrated that protein bands of approximately 95- (Fig. 2A filled arrowhead) and 80-kDa (Fig. 2A open arrowhead) were specifically detected in the WT but not the KO parasites confirming that the bands identified were specific for PfMSPDBL1. Identification and size of the bands identified was in agreement with previously published results [17]. Preimmune serum did not recognize the native PfMSPDBL1 protein in the lysate of WT parasite (data not shown). To ensure that the same amount of each parasite protein sample was loaded in each lane for Western blot analysis, the membranes were also probed with anti-PfHSP70 monoclonal antibody (4C9) [27]. The intensities of the PfHSP70 bands indicated that the amounts of samples loaded in the lanes were comparable (Fig. 2A, bottom panel). These results suggest that the rFL prepared by the cell-free system retained native epitopes and confirm that anti-rFL serum recognized the native PfMSPDBL1 protein in the 3D7 parasite.

3.3. Anti-PfMSPDBL1 antibodies do not cross-react with conserved SPAM domains of other MSP3 family members

Because Singh et al. [18] showed that antibodies against the SPAM domain of the MSP3 family cross-reacts to SPAM domains of other members in MSP3 family, the 100-kDa signal detected in both WT and KO parasites (Fig. 2A arrow) may represent cross-reaction with an unknown MSP3 family member. Therefore we investigated the possibility of the cross-reaction of anti-rFL serum to other SPAM domains of the family. To do this, N-terminal hexa-His-tagged recombinant proteins of all the conserved SPAM domains of the MSP3 family members were synthesized using the wheat germ cell-free system and Ni-affinity purified. The amino acid sequences of different recombinant SPAM domains (Fig. 2B) synthesized by us in this study were identical to that of the respective recombinant SPAM domains synthesized in the previous study [18]. The syntheses of recombinant proteins were confirmed by Coomassie Brilliant Blue staining (Fig. 2B) or anti-His antibody probing in western blotting (second panel of Fig. 2C). To validate antigenicity of the proteins, the SPAM proteins were probed with pooled malaria immune sera (bottom panel of Fig. 2C), or pooled naïve sera from Thailand (third panel of Fig. 2C). All of them reacted to the immune sera (bottom panel of Fig. 2C), but not to the naïve sera (third panel of Fig. 2C), suggesting that all of the recombinant SPAM domains possess correct conformation. However, when these proteins were probed with anti-rFL rabbit serum, none of them except SPAM domain of PfMSPDBL1 reacted against anti-rFL serum indicating that the anti-rFL serum do not cross-react with other conserved SPAM domains of the MSP3 family members, in other words anti-rFL serum react specifically to SPAM domain of PfMSPDBL1 (lane "MSP3.4" in top panel of Fig. 2C).

3.4. Native PfMSPDBL1 is localized on the merozoite surface

Although merozoite surface localization of the GFP-fused PfMSPDBL1 protein was previously reported using transgenic parasites [17,28], localization of the native PfMSPDBL1 protein in the parasite, especially free merozoites, has never been confirmed to date. In order to determine the localization of the native PfMSPDBL1 protein in 3D7 wild type mature schizonts and free merozoites, IFA was carried out using anti-rFL and -PfMSP1$_{19}$ sera. In mature schizonts, the PfMSPDBL1 was localized to the circumference of each merozoites (upper panels of Fig. 3). To confirm the surface localization of PfMSPDBL1, we observed the free merozoites that were not permeabilized with Triton X-100. The PfMSPDBL1 was detected on the surface of free merozoites and it was seen to colocalize with PfMSP1 (bottom panels of Fig. 3). On the other hand, under this non-permeabilization condition, the cytoplasmic protein PfHSP70 [probed with anti-PfHSP70 monoclonal antibody (4C9)] was not detected (data not shown), indicating that the parasite plasma membrane is intact. Additionally, in ring and trophozoite stage parasites, PfMSPDBL1 was not detected (data not shown). These results demonstrated for the first time that the native PfMSPDBL1 is localized on the surface of free merozoites and it suggests that it is exposed to human immune system (i.e., neutralizing antibodies).

3.5. Anti-PfMSPDBL1 antibodies specifically inhibit merozoite invasion into erythrocytes

To investigate whether anti-rFL antibodies block parasite invasion into erythrocyte, growth inhibition assays were carried out using 3D7 parasites. Anti-AMA1 and -GST IgGs [29,30] were used as a positive and a negative control, respectively. Anti-AMA1 and -GST IgGs inhibited growth by 57% and 5% respectively. Upon culturing parasites with anti-rFL IgG, parasite growth was significantly inhibited (37% inhibition) when compared with anti-GST IgG ($p < 0.001$, Fig. 4A). Moreover, the inhibitory activity of anti-rFL IgG is dose-dependent (Fig. 4B). To test the effects of IgGs on growth per se and not on invasion, the IgGs were added to ring stage parasites at 0.2–0.4% initial parasitemia. After 24–30 h the numbers of intra-erythrocytic parasites (i.e., trophozoites, early schizonts, and late schizonts) were counted. The results showed that among the groups neither total percent growth nor percentage of different stages (i.e., trophozoite, early schizont, and late schizont) were significantly different when the parasites were grown in presence of different IgGs ($p > 0.05$, Fig. 4C). Taken together, anti-rFL IgG inhibits merozoite invasion into erythrocytes but not parasite growth.

To confirm the specificity of the inhibitory activity of the anti-rFL IgG, growth inhibition assays were carried out using the 3D7ΔDBL1 parasite. Before the assay was performed, we compared the invasion efficiency of both wild type 3D7 (WT) and the 3D7ΔDBL1 (KO) parasites (Fig. 4D). Although parasitemia of the 3D7ΔDBL1 was slightly lower than that of the 3D7 wild type parasite after the 30 h observation, the difference in the % parasitemia was not statistically significant (Fig. 4D). Consistent with the data in Fig. 4A, anti-AMA1 IgG significantly inhibited 3D7ΔDBL1 parasite invasion by 50% when compared with anti-GST ($p < 0.001$, Fig. 4E). In contrast, no inhibitory activity of anti-rFL IgG (2% inhibition) was observed when compared with anti-GST ($p > 0.05$). These results indicate that the inhibitory activity of anti-rFL IgG was specific to PfSMSPDBL1 protein.

In order to determine the region of the rFL that is targeted by the inhibitory antibodies, the GIA was performed using anti-rFL IgG that was pre-incubated with either rFL or rSPAM protein. Anti-rFL and -GST IgGs without pre-incubation were used as a positive and a negative control, respectively, and rGST protein was used as a negative control for the pre-incubation. Before performing this assay, we confirmed that all recombinant proteins (final concentration at 0.2 mg/ml) did not have an inhibitory effect on parasite growth (Fig. 5A). As shown in Fig. 5B, the pre-incubation of anti-rFL IgG with rFL protein completely abolished the inhibitory activity of anti-rFL IgG (0% inhibition). Moreover, effect of the pre-incubation on inhibitory activity of anti-rFL IgG was dose-dependent (Fig. 5C). In contrast, pre-incubation of anti-rFL IgG with either rSPAM (32% inhibition) or rGST proteins (30% inhibition) did not reduce the inhibitory activity of anti-rFL IgG (33% inhibition) ($p > 0.05$, Fig. 5B). Taken together, these results suggest that the invasion inhibitory antibodies targets specifically PfMSPDBL1 protein or rather the region of PfMSPDBL1 other than the SPAM domain, and that the antibodies against the SPAM domain did not contribute to the invasion inhibitory activity of anti-rFL IgG.

3.6. Antibodies to PfMSPDBL1 were elicited in malaria immune individuals

Since the anti-rFL antibody showed the invasion inhibitory activity, it is important to determine whether PfMSPDBL1 is immunogenic in humans. In order to determine the antibody responses against PfMSPDBL1, serum samples from individuals living in a *P. falciparum* endemic area in Thailand were tested against rFL as capture antigen in ELISA. Malaria naïve human serum samples obtained from individuals living in Bangkok, Thailand were used as a negative control. As shown in Fig. 6, antibody titer against rFL of PfMSPDBL1 was significantly higher in asymptomatic malaria immune sera than in naïve group ($p < 0.001$), suggesting that PfMSPDBL1 was immunogenic to humans.

4. Discussion

The striking feature of the PfMSPDBL1 protein is the presence of both DBL and SPAM domains. The well-characterized merozoite

proteins with DBL domains, such as EBA175, are known to play crucial roles in erythrocyte invasion [7]. On the other hand, the proteins with SPAM domains, such as MSP3, are targets of protective immune response [31,32]. The aim of this study was to investigate the effects of antibodies against PfMSPDBL1 protein, which has both DBL and SPAM, on merozoite invasion of erythrocytes. Here we report for the first time that PfMSPDBL1 specific antibodies inhibit *P. falciparum* invasion of erythrocytes, and that the inhibitory effect of anti-PfMSPDBL1 antibodies was not conferred by any cross-reaction to SPAM domains of other MSP3 family members. While the previous study has shown that SPAM domains of the MSP3 family members, including PfMSPDBL1, was a target for monocyte-dependent invasion inhibitory activity of antibodies (i.e., ADCI assay) [18], we have shown here that the regions other than the SPAM domain of PfMSPDBL1 was the target of the monocyte-independent invasion inhibitory activity of rFL of PfMSPDBL1 antibodies.

Singh et al. [18] proposed a new multigene family, MSP3 family, which consists of MSP3 (MSP3.1: encoded by PF10_0345 gene), MSP6 (MSP3.2: encoded by PF10_0346 gene), H101 (MSP3.3: encoded by PF10_0347 gene), MSPDBL1 (MSP3.4: encoded by PF10_0348 gene), H103 (MSP11 or MSP3.7: encoded by PF10_0352 gene) and MSPDBL2 (MSP3.8: encoded by PF10_0355 gene). Owing to the high amino acid sequence conservation among the SPAM domains of MSP3 family members, both antibodies purified from hyperimmune human adults or mouse antisera against each SPAM domain demonstrated significant cross-reactivity with SPAM domains of MSP family members [18,33]. However, our anti-rFL rabbit antibodies did not cross-react to SPAM domains of any other MSP3 family members (Fig. 2C). Although we do not know why our data is different from the previous studies [18,33], the plausible explanations might be the difference in protein expression system employed which affects the folding of the recombinant proteins, and the difference in the region used for immunization. Further studies are needed to solve the conundrum. Since we could obtain PfMSPDBL1 specific anti-rFL antibodies, we were able to investigate the specific role of PfMSPDBL1 in parasite invasion and growth.

The growth of the 3D7ΔDBL1 parasite (Uboldi et al., in preparation) was compared to that of 3D7 wild type (Fig. 4D), indicating that PfMSPDBL1 proteins was not essential for the blood-stage life cycle and presumably its function could be compensated by another protein(s). Such compensation is a general phenomenon among erythrocyte binding ligand proteins of *P. falciparum* such as EBAs [7]. Functional compensation was thought to be an issue for their potential as a blood-stage malaria vaccine to date [6]. In spite of the fact that PfMSPDBL1 was not essential for blood stage parasite growth (Uboldi et al., in preparation), our data indicates that the anti-rFL antibodies alone, without combination of antibodies against the other MSP3 family members, effectively inhibited the wild type parasite (which expresses non-essential PfMSPDBL1) invasion into erythrocytes, but not growth (Fig. 4A–C). Moreover the *pfmspdbdl1* gene disruption completely abolished the inhibitory activity of anti-rFL antibodies (Fig. 4E), confirming that the invasion inhibitory effect of anti-rFL antibodies is completely specific to the PfMSPDBL1 protein. These results suggest that the PfMSPDBL1 may be a potential blood-stage vaccine candidate.

To search for the region of PfMSPDBL1 that was targeted by the inhibitory anti-rFL antibodies, growth inhibition assays were done using anti-rFL antibodies that pre-incubated with either rFL or rSPAM protein. Although rFL protein completely neutralized the inhibitory activity of anti-rFL antibodies, rSPAM protein did not (Fig. 5B and C), suggesting that the SPAM domain did not contain target epitopes of the inhibitory anti-rFL antibodies. These results highlight regions other than the SPAM domain as a target of invasion inhibition of the anti-PfMSPDBL1 antibodies. Thus we have attempted to produce recombinant DBL domain of PfMSPDBL1 for neutralization assays and antibody production, however we have not been able to synthesize the DBL protein to date. Although further studies will be necessary, we speculate that the DBL domain maybe the target of the inhibitory activity of anti-rFL antibodies as well as DBL domains of other EBAs [34–36]. Moreover, this possibility is supported by the reported findings on the binding capacity of the DBL domain of PfMSPDBL1 to human erythrocytes determined using a COS cell assay [17]. Taken together, in addition to the ADCI based parasite growth inhibition targeting SPAM domains within the MSP3 family [18,33], antibodies against the region other than SPAM domain confers invasion inhibition. Thus the PfMSPDBL1 with both DBL and SPAM domains is a promising blood-stage vaccine candidate of *P. falciparum*.

We demonstrated that native PfMSPDBL1 protein was located on the merozoite surface. Previous studies have used GFP-fused PfMSPDBL1 proteins that were under the control of *pfama1* or *pfmsp2* gene promoter [17,28], therefore, it cannot be ruled out that this may have caused some mislocalization and overexpression thus perturbing the natural PfMSPDBL1 localization. In this study, for the first time the clear localization of native PfMSPDBL1 was on the surface of merozoites observed using the 3D7 wild type parasites (Fig. 3), supporting the potential role of PfMSPDBL1 on initial attachment in the erythrocyte invasion process of merozoites and the possibility of PfMSPDBL1 being recognized by human immune system. It has been previously demonstrated that antibodies against the conserved SPAM of PfMSPDBL1 is highly prevalent among hyperimmune adults living in Senegal [33]. In addition, Wickramarachchi et al. [17] showed that both the DBL and SPAM domains were recognized by immune sera from individuals living in India. In this study, antibodies against PfMSPDBL1 was also elicited among asymptomatic immune adults living in endemic area in Thailand (Fig. 6), suggesting antibodies against PfMSPDBL1 can generally be induced irrespective of malaria endemic areas and parasite isolates. Therefore further sero-epidemiological studies on PfMSPDBL1 should be implemented on a global scale to ensure a positive correlation between anti-PfMSPDBL1 antibodies titer and clinical protection on malaria.

In conclusion, we demonstrated for the first time that anti-PfMSPDBL1 specific antibodies can inhibit merozoite invasion into erythrocytes of *P. falciparum*, however the anti-SPAM domain antibodies are not involved in the inhibition. Therefore the region other than SPAM domain, including DBL domain in PfMSPDBL1 may be the target for the invasion inhibitory antibodies against rFL antigen. Although further studies are necessary to validate that the DBL domain of PfMSPDBL1 as the potential target for invasion inhibition, this work serves as the first step towards elucidating the vaccine candidacy of PfMSPDBL1.

Acknowledgments

We are grateful to Guy A. Schiehser, David Jacobus, and Walter Reed Army Institute of Research for the drug WR99210. We thank Thangavelu U. Arumugam for the critical reading of the manuscript and Daisuke Ito for the technical assistance. We also thank the Japanese Red Cross Society for providing us the human erythrocytes and human plasma. AGM is an ARC Australian Research Fellow. The work performed at WEHI was made possible through Victorian State Government Operational Infrastructure Support and Australian Government NHMRC IRIISS.

This research was supported in part by grants from The Bill and Melinda Gates Foundation, from the Ministry of Education, Culture, Sports, Science and Technology (21249028, 21022034, 23406007, and 23117008), and from the Ministry of Health, Labour, and Welfare, Japan (H21-Chikyukibo-ippan-005).

References

[1] WHO. World Malaria Report 2010; 2010 [cited; Available from: http://www.who.int/malaria/world_malaria_report_2010/en/index.html.

[2] Langhorne J, Ndungu FM, Sponaas AM, Marsh K. Immunity to malaria: more questions than answers. Nat Immunol 2008;9(July (7)):725–32.

[3] Cohen S, McGregor IA, Carrington S. Gamma-globulin and acquired immunity to human malaria. Nature 1961;192(November):733–7.

[4] Sabchareon A, Burnouf T, Ouattara D, Attanath P, Bouharoun-Tayoun H, Chantavanich P, et al. Parasitologic and clinical human response to immunoglobulin administration in falciparum malaria. Am J Trop Med Hyg 1991;45(September (3)):297–308.

[5] Crompton PD, Pierce SK, Miller LH. Advances and challenges in malaria vaccine development. J Clin Invest 2010;120(December (12)):4168–78.

[6] Greenwood BM, Targett GA. Malaria vaccines and the new malaria agenda. Clin Microbiol Infect 2011;17(November (11)):1600–7.

[7] Cowman AF, Crabb BS. Invasion of red blood cells by malaria parasites. Cell 2006;124(February (4)):755–66.

[8] Iyer J, Grüner AC, Rénia L, Snounou G, Preiser PR. Invasion of host cells by malaria parasites: a tale of two protein families. Mol Microbiol 2007;65(July (2)):231–49.

[9] Thompson JK, Triglia T, Reed MB, Cowman AF. A novel ligand from *Plasmodium falciparum* that binds to a sialic acid-containing receptor on the surface of human erythrocytes. Mol Microbiol 2001;41(July (1)):47–58.

[10] Gilberger TW, Thompson JK, Triglia T, Good RT, Duraisingh MT, Cowman AF. A novel erythrocyte binding antigen-175 paralogue from *Plasmodium falciparum* defines a new trypsin-resistant receptor on human erythrocytes. J Biol Chem 2003;278(April (16)):14480–6.

[11] Singh S, Alam MM, Pal-Bhowmick I, Brzostowski JA, Chitnis CE. Distinct external signals trigger sequential release of apical organelles during erythrocyte invasion by malaria parasites. PLoS Pathog 2010;6(February (2)):e1000746.

[12] Cohen S, Butcher GA, Crandall RB. Action of malarial antibody in vitro. Nature 1969;223(July (5204)):368–71.

[13] Brown GV, Anders RF, Mitchell GF, Heywood PF. Target antigens of purified human immunoglobulins which inhibit growth of *Plasmodium falciparum* in vitro. Nature 1982;297(June (5867)):591–3.

[14] McCallum FJ, Persson KE, Mugyenyi CK, Fowkes FJ, Simpson JA, Richards JS, et al. Acquisition of growth-inhibitory antibodies against blood-stage *Plasmodium falciparum*. PLoS One 2008;3(10):e3571.

[15] Bouharoun-Tayoun H, Attanath P, Sabchareon A, Chongsuphajaisiddhi T, Druilhe P. Antibodies that protect humans against *Plasmodium falciparum* blood stages do not on their own inhibit parasite growth and invasion in vitro, but act in cooperation with monocytes. J Exp Med 1990;172(December (6)): 1633–41.

[16] Richards JS, Beeson JG. The future for blood-stage vaccines against malaria. Immunol Cell Biol 2009;87(July (5)):377–90.

[17] Wickramarachchi T, Cabrera AL, Sinha D, Dhawan S, Chandran T, Devi YS, et al. A novel *Plasmodium falciparum* erythrocyte binding protein associated with the merozoite surface, PfDBLMSP. Int J Parasitol 2009;39(January (7)): 763–73.

[18] Singh S, Soe S, Weisman S, Barnwell JW, Pérignon JL, Druilhe P. A conserved multi-gene family induces cross-reactive antibodies effective in defense against *Plasmodium falciparum*. PLoS One 2009;4(4):e5410.

[19] Kamura N, Sawasaki T, Kasahara Y, Takai K, Endo Y. Selection of 5′-untranslated sequences that enhance initiation of translation in a cell-free protein synthesis system from wheat embryos. Bioorg Med Chem Lett 2005;15(December (24)):5402–6.

[20] Tsuboi T, Takeo S, Iriko H, Jin L, Tsuchimochi M, Matsuda S, et al. Wheat germ cell-free system-based production of malaria proteins for discovery of novel vaccine candidates. Infect Immun 2008;76(April (4)):1702–8.

[21] Tsuboi T, Takeo S, Sawasaki T, Torii M, Endo Y. An efficient approach to the production of vaccines against the malaria parasite. Methods Mol Biol 2010;607:73–83.

[22] Tsuboi T, Takeo S, Arumugam TU, Otsuki H, Torii M. The wheat germ cell-free protein synthesis system: a key tool for novel malaria vaccine candidate discovery. Acta Trop 2010;114(June (3)):171–6.

[23] Takeo S, Arumugam TU, Torii M, Tsuboi T. Wheat germ cell-free technology for accelerating the malaria vaccine research. Expert Opin Drug Discov 2009;4(November (11)):1191–9.

[24] Trager W, Jensen JB. Human malaria parasites in continuous culture. Science 1976;193(August (4254)):673–5.

[25] Coleman RE, Maneechai N, Rachaphaew N, Kumpitak C, Miller RS, Soyseng V, et al. Comparison of field and expert laboratory microscopy for active surveillance for asymptomatic *Plasmodium falciparum* and *Plasmodium vivax* in western Thailand. Am J Trop Med Hyg 2002;67(August (2)):141–4.

[26] Coleman RE, Kumpitak C, Ponlawat A, Maneechai N, Phunkitchar V, Rachapaew N, et al. Infectivity of asymptomatic *Plasmodium*-infected human populations to Anopheles dirus mosquitoes in western Thailand. J Med Entomol 2004;41(March (2)):201–8.

[27] Tsuji M, Mattei D, Nussenzweig RS, Eichinger D, Zavala F. Demonstration of heat-shock protein 70 in the sporozoite stage of malaria parasites. Parasitol Res 1994;80(1):16–21.

[28] Hu G, Cabrera A, Kono M, Mok S, Chaal BK, Haase S, et al. Transcriptional profiling of growth perturbations of the human malaria parasite *Plasmodium falciparum*. Nat Biotechnol 2010;28(January (1)):91–8.

[29] Ito D, Han ET, Takeo S, Thongkukiatkul A, Otsuki H, Torii M, et al. Plasmodial ortholog of *Toxoplasma gondii* rhoptry neck protein 3 is localized to the rhoptry body. Parasitol Int 2011;60(June (2)):132–8.

[30] Arumugam TU, Takeo S, Yamasaki T, Thonkukiatkul A, Miura K, Otsuki H, et al. Discovery of GAMA, a *Plasmodium falciparum* merozoite micronemal protein, as a novel blood-stage vaccine candidate antigen. Infect Immun 2011;79(November (11)):4523–32.

[31] Druilhe P, Spertini F, Soesoe D, Corradin G, Mejia P, Singh S, et al. A malaria vaccine that elicits in humans antibodies able to kill *Plasmodium falciparum*. PLoS Med 2005;2(November (11)):e344.

[32] Roussilhon C, Oeuvray C, Müller-Graf C, Tall A, Rogier C, Trape JF, et al. Long-term clinical protection from falciparum malaria is strongly associated with IgG3 antibodies to merozoite surface protein 3. PLoS Med 2007;4(November (11)):e320.

[33] Demanga CG, Daher LJ, Prieur E, Blanc C, Pérignon JL, Bouharoun-Tayoun H, et al. Toward the rational design of a malaria vaccine construct using the MSP3 family as an example: contribution of antigenicity studies in humans. Infect Immun 2010;78(January (1)):486–94.

[34] Grimberg BT, Udomsangpetch R, Xainli J, McHenry A, Panichakul T, Sattabongkot J, et al. Plasmodium vivax invasion of human erythrocytes inhibited by antibodies directed against the Duffy binding protein. PLoS Med 2007;4(December (12)):e337.

[35] Pandey KC, Singh S, Pattnaik P, Pillai CR, Pillai U, Lynn A, et al. Bacterially expressed and refolded receptor binding domain of *Plasmodium falciparum* EBA-175 elicits invasion inhibitory antibodies. Mol Biochem Parasitol 2002;123(August (1)):23–33.

[36] Jiang L, Gaur D, Mu J, Zhou H, Long CA, Miller LH. Evidence for erythrocyte-binding antigen 175 as a component of a ligand-blocking blood-stage malaria vaccine. Proc Natl Acad Sci USA 2011;108(May (18)):7553–8.

THE JOURNAL OF BIOLOGICAL CHEMISTRY VOL. 287, NO. 11, pp. 7871–7884, March 9, 2012

Biosynthesis, Localization, and Macromolecular Arrangement of the *Plasmodium falciparum* Translocon of Exported Proteins (PTEX)*[S]

Received for publication, November 28, 2011, and in revised form, January 12, 2012 Published, JBC Papers in Press, January 17, 2012, DOI 10.1074/jbc.M111.328591

Hayley E. Bullen,[a,b] Sarah C. Charnaud,[a,c] Ming Kalanon,[d] David T. Riglar,[b,e1] Chaitali Dekiwadia,[f] Niwat Kangwanrangsan,[g] Motomi Torii,[g] Takafumi Tsuboi,[h] Jacob Baum,[e] Stuart A. Ralph,[f] Alan F. Cowman,[e] Tania F. de Koning-Ward,[d2] Brendan S. Crabb,[a,i,j3] and Paul R. Gilson[a,j4]

From the [a]Macfarlane Burnet Institute for Medical Research and Public Health, Melbourne, Victoria 3004, Australia, the [b]Department of Medical Biology, The University of Melbourne, Melbourne, Victoria 3010, Australia, the [c]Faculty of Medicine, Nursing and Health Sciences, Monash University, Victoria 3800, Australia, the [d]School of Medicine, Deakin University, Geelong, Victoria 3216, [e]Infection and Immunity Division, The Walter and Eliza Hall Institute, Melbourne, Victoria 3052, [f]Bio21 Molecular Science and Biotechnology Institute, The University of Melbourne, Victoria 3010, Australia, the [g]Department of Molecular Parasitology, Ehime University Graduate School of Medicine, Toon, Ehime 791-0295, Japan, [h]Cell-Free Science and Technology Research Center and Venture Business Laboratory, Ehime University, Matsuyama, Ehime 790-8577, Japan, the [i]Department of Microbiology and Immunology, The University of Melbourne, Victoria 3010, Australia, and the [j]Department of Immunology, Monash University, Victoria 3800, Australia

Background: To survive, *Plasmodium falciparum* parasites export proteins into their host cell.
Results: We have characterized the localization, synthesis, and macromolecular-arrangement of the protein export machinery in *Plasmodium falciparum.*
Conclusion: This machinery is carried into the host-cell and is present as a large macromolecular complex.
Significance: These data fill current gaps in the field relating to the biochemical nature of *Plasmodium falciparum* protein export.

To survive within its host erythrocyte, *Plasmodium falciparum* must export hundreds of proteins across both its parasite plasma membrane and surrounding parasitophorous vacuole membrane, most of which are likely to use a protein complex known as PTEX (*Plasmodium* translocon of exported proteins). PTEX is a putative protein trafficking machinery responsible for the export of hundreds of proteins across the parasitophorous vacuole membrane and into the human host cell. Five proteins are known to comprise the PTEX complex, and in this study, three of the major stoichiometric components are investigated including HSP101 (a AAA^+ ATPase), a protein of no known function termed PTEX150, and the apparent membrane component EXP2. We show that these proteins are synthesized in the preceding schizont stage (PTEX150 and HSP101) or even earlier in the life cycle (EXP2), and before invasion these components reside within the dense granules of invasive merozoites. From these apical organelles, the protein complex is released into the host cell where it resides with little turnover in the parasitophorous vacuole membrane for most of the remainder of the following cell cycle. At this membrane, PTEX is arranged in a stable macromolecular complex of >1230 kDa that includes an ~600-kDa apparently homo-oligomeric complex of EXP2 that can be separated from the remainder of the PTEX complex using non-ionic detergents. Two different biochemical methods undertaken here suggest that PTEX components associate as EXP2-PTEX150-HSP101, with EXP2 associating with the vacuolar membrane. Collectively, these data support the hypothesis that EXP2 oligomerizes and potentially forms the putative membrane-spanning pore to which the remainder of the PTEX complex is attached.

Malaria remains one of mankind's greatest health challenges. The causative agents of this disease are protozoan parasites belonging to the genus *Plasmodium,* which during invasion of their host erythrocyte become encased within a parasitophorous vacuole membrane (PVM).[5] In what is considered to be a crucial aspect of parasite pathogenesis and survival, the human malaria parasite *Plasmodium falciparum* exports hundreds of proteins across the PVM into the erythrocyte cytosol (1–3). The mechanisms by which proteins destined for export are trafficked from their endoplasmic reticulum origins to their final destination within the host cell cytosol have been extensively investigated in recent years (4). Within this paper we

* This work was supported by Australian National Health and Medical Research Council Grants 516740, 533811, and 406601).
[S] This article contains supplemental Table 1 and Figs. 1 and 2.
[1] Supported by a Pratt Foundation Scholarship through University of Melbourne.
[2] Supported by a National Health and Medical Research Council Career Development Fellowship award.
[3] To whom correspondence may be addressed: The Burnet Institute, 85 Commercial Rd., Melbourne, VIC 3004, Australia. E-mail: crabb@burnet.edu.au.
[4] To whom correspondence may be addressed: The Burnet Institute, 85 Commercial Rd., Melbourne, VIC 3004, Australia. E-mail: gilson@burnet.edu.au.

[5] The abbreviations used are: PVM, parasitophorous vacuole (PV) membrane; PTEX, *Plasmodium* translocon of exported protein; BN, Blue Native; DSP, dithiobis(succinimidyl propionate); TRX2, thioredoxin; EXP2, exported protein 2; bis-tris, 2-[bis(2-hydroxyethyl)amino]-2-(hydroxymethyl)propane-1,3-diol; RIPA, radioimmune precipitation assay buffer; RESA, ring-infected erythrocyte surface antigen.

investigate the biochemical characteristics of a key component of this export pathway, the plasmodium translocon of exported proteins (PTEX) (5). This proteinaceous complex resides at the PVM and is considered to provide the most likely means by which parasite-derived proteins cross the PVM and enter the erythrocyte cytosol.

Definitive proof of PTEX functioning as a protein-exporting translocon is currently lacking; however, despite this the constituent parts of this complex have been shown to specifically bind exported proteins and satisfy many criteria expected for such a machinery. First, one of the five proteins comprising PTEX, HSP101, is a AAA^+ ATPase chaperone that hydrolases ATP to putatively unfold protein cargo before driving it across the PVM. HSP101 is, therefore, likely to function similarly although in the reverse direction to the related ClpC chaperone found in plant and algal chloroplasts, which is used by the Tic/Toc protein translocon system to import proteins into this organelle (6). The other PTEX components are a thioredoxin (TRX2), Exported Protein 2 (EXP2), and two hypothetical proteins termed PTEX150 and PTEX88, so named because of the size they migrate at by SDS-PAGE (5). These latter two proteins have no conserved domains diagnostic of putative function, and thus their roles within the complex remain unknown. Each of these components is, however, unique to the *Plasmodium* genus.

To enable passage of exported proteins across the PVM, it is assumed that PTEX contains a membrane-spanning channel. Although immunofluorescence microscopy and differential solubilization of infected erythrocytes has indicated that PTEX resides at the PVM (5), none of its proteins possess classic transmembrane domains. EXP2 is, however, emerging as a possible candidate for this putative role. Experiments with schizont-stage parasites have shown that EXP2 resists extraction from membrane fractions in high salt (7) and associates strongly with the carbonate-insoluble fraction during carbonate extraction (5, 7). Recently, modeling of the predicted structure of EXP2 strengthened its putative membrane provenance by predicting similarity with the α-pore-forming toxin of *Escherichia coli*, HlyE (5), which has been shown to form a dodecameric 12-mer or 13-mer pore within host cell membranes (8–11). Subsequently, it is of particular interest if EXP2 can oligomerize to form a protein-translocating pore within the PVM.

Here we investigate the biosynthesis, localization, and macromolecular arrangement of the PTEX complex. We show that three of the major PTEX components (EXP2, HSP101, and PTEX150) are present in the dense granules of extracellular merozoites before invasion and are released into the newly formed PVM. Interestingly, we have found that whereas HSP101 and PTEX150 are translated in schizonts, EXP2 is made earlier in the erythrocytic cycle; thus, expression of these translocon components does not appear to be co-regulated despite ending up in the same localities of the dense granules and ring-stage PVM. We show that PTEX is present as a >1230-kDa complex containing an ~600-kDa EXP2 homo-oligomeric species, of which a dimer is likely to be the core subunit. EXP2 is the most strongly membrane-associated PTEX component throughout the intraerythrocytic life cycle, conducive with it forming a membrane pore. Last, we provide evidence that the PTEX components associate at the PVM via EXP2-PTEX150-HSP101. Collectively, data shown here are consistent with EXP2 potentially forming a membrane-associated pore to which the remainder of the large PTEX complex is attached.

EXPERIMENTAL PROCEDURES

Continuous Culturing of P. falciparum—Blood stage *P. falciparum* 3D7 parasites transfected with plasmid constructs outlined in de Koning-Ward *et al.* (5) were cultured continuously as previously described (12). Parasite strains D10 and D10 PfM3′ parasites (13) were similarly cultured.

Freeze/Thaw Preparation of Parasite Pellets—Infected erythrocytes were pelleted (3750 rpm/10 min), snap-frozen in dry ice, and subsequently thawed at room temperature. This was repeated 5 times before re-pelleting (7000 × *g* for 1min) and gentle rinsing in PBS until excess hemoglobin was removed.

Recombinant EXP2 Protein Expression—The EXP2 (PF14_0678) fragment (73–864 bp) encoding Asp-25 to Glu-287 was cloned into the XhoI/BamHI sites of the vector pEU-E01-GST-TEV-N2 specifically designed for the wheat germ cell-free protein expression system (CellFree Sciences, Matsuyama, Japan) (14). The GST fusion EXP2 fragment was expressed in a wheat germ cell-free expression system (CellFree Sciences) and was purified by passing the supernatant through the glutathione-Sepharose 4B column (GE Healthcare) followed by tobacco etch virus protease (Invitrogen) cleavage to remove the GST tag (15). Concentration of affinity-purified EXP2 protein was determined using the Bradford protein assay kit (Bio-Rad). Rabbit antiserum was raised to recombinant EXP2 after standard protocols at The Walter and Eliza Hall Institute Monoclonal Facility.

Immunofluorescence Assays—Infected erythrocytes were either smeared onto slides and fixed in ice-cold methanol for 5 mins before blocking in 1% casein, or invading purified merozoites (16) were pelleted (2000 × *g* for 2 min) and washed in PBS before fixation in 4% paraformaldehyde, 0.0075% glutaraldehyde, PBS as outlined in Tonkin *et al.* (17) before blocking in BSA. Cells were probed with rabbit anti-EXP2 (50 μg/ml), rabbit anti-HSP101 (80 μg/ml), anti-RESA mAb 1812 (20 μg/ml), anti-AMA1 mAb 1F9 (25 μg/ml; both RESA and AMA1 mAbs were kind gifts from Robin Anders), anti-Rap1 mAb 7H8150 (35 μg/ml), and rabbit anti-RON4 (2.6 μg/ml) and then labeled with AlexaFluor secondary antibodies (1:2000) for 1 h before mounting in Vectashield with DAPI (Vector). All imaging was completed on a Zeiss Axio Observer Z1 using Axiovision software. Deconvolution of images was performed with Huygens Deconvolution Image platform using default settings and the parameters obtained from the Axiovision zvi file. Pearson's colocalization coefficients were calculated with the JACoP ImageJ plugin, and images were manipulated with ImageJ and Photoshop.

Immunoelectron Microscopy—Merozoites used for immunoelectron microscopy were prepared as described previously (16). Briefly, synchronous, magnetically-purified D10 and PTEX150-HA (5) late schizonts were treated with 10 μM E64 protease inhibitor for 6–8 h. Unfiltered D10 parasites were collected at this point. Filtered merozoites were obtained by

filtration through a pre-wet 1.2-μm Acrodisc 32-mm syringe filter. Merozoites were fixed with 1% glutaraldehyde, 30 min on ice. Fixed cells were pelleted (20,000 × *g* for 1 min) and washed 3 times in ice-cold PBS, equilibrated into water, deposited into low melting point agarose, dehydrated in ethanol, and embedded in LR gold resin (ProSciTech) that was polymerized with benzoyl peroxide (SPI-Chem). 100-nm sections were obtained with an Ultracut R ultramicrotome (Leica) and labeled with rabbit anti-EXP2 (20 μg/ml) or anti-HA mAb (0.7 μg/ml 12CA5, Roche Applied Science) followed by anti-rabbit and mouse IgGs conjugated to 18-nm gold (1:20, Jackson ImmunoResearch). The sections were then post-stained and observed at 120 kV on a CM120 BioTWIN transmission electron microscope (Philips).

Blue Native PAGE Analysis—Mixed stage *P. falciparum* parasites were saponin-lysed and resuspended in Triton X-100 with mixing at 4 °C/30 min. Insoluble material was pelleted (14,000 × *g* for 30 min at 4 °C), and supernatant fractions were collected. Samples were electrophoresed and transferred to PVDF as per the manufacturer instructions (Invitrogen). Blots were blocked in 1% casein in PBS and probed with either rabbit anti-EXP2 (5 μg/ml), mouse anti-EXP2 (mAb 7.7, 5 μg/ml, a kind gift from Drs Jana McBride and David Cavanagh (7)), rabbit anti-HSP101 (10 μg/ml) (5), rabbit anti-PTEX150 (10 μg/ml) (5), mouse anti-HA (mAb 12CA5, 10 μg/ml), or chicken anti-HA (1:1000, Abcam). Fluorescent secondary antibodies were from Rockland Immunochemicals. Bound antibody probes were detected with LiCor Odyssey Fc infrared imager followed by analysis with Odyssey v1.2 software.

Pulse-Chase Analysis—PTEX150-HA or HSP101-HA parasites (~6% parasitemia) were sorbitol-synchronized and grown to either 38–42 h schizonts or 4–8 h rings and rinsed in methionine/cysteine-free media. 200 μCi/ml ^{35}S (Easytag Expre^{35}S^{35}S cysteine/methionine) was added and pulsed for 1 h. Parasites were pelleted (1200 × *g* for 5 min), and ^{35}S was removed by washing twice in standard RPMI-HEPES media. Cleaned cells were resuspended in 25 ml of 4% hematocrit RPMI-HEPES media, and a 5-ml sample was taken immediately (time point 0) and every subsequent 12 h for a total 48 h. All samples were frozen at −80 °C, and upon thawing, samples were incubated in equal volume 2% Triton X-100 with Complete protease inhibitors (Roche Applied Science) for 6 h at room temperature. Lysate was cleared (3750 rpm for 15 min), and 50 μl of goat polyclonal anti-HA beads (Abcam) was added overnight at 4 °C. After washing, bound proteins were eluted in 75 μl of 1× NRSB (0.05 M Tris-HCl, pH 6.8, 10% glycerol, 2 mM EDTA, 2% SDS, bromphenol blue) before electrophoretic separation and subsequent Western blotting. After blocking in 1% casein, blots were probed with chicken anti-HA, rabbit anti-EXP2, rabbit anti-HSP101 (5), or rabbit anti-PTEX150 (5) overnight at 4 °C before imaging using the Odyssey Fc imaging system. Blots were subsequently air-dried and exposed to a Typhoon PhosphorImager (GE Healthcare) cassette for 14 days before imaging.

Chemical Cross-linking—*P. falciparum* mixed stage parasites were harvested, and whole infected erythrocytes were cross-linked using dithiobis(succinimidyl propionate) (DSP) as previously described (18). Cells were subsequently saponin-lysed and resuspended in 1× NRSB. 0, 3, 6, 20, 60, or 200 mM DTT was titrated in before incubation at 80 °C for 5 min. Samples were electrophoresed and Western-blotted.

Affinity Purification Assays Using Chemical Cross-linking—Mixed stage PTEX150-HA parasites were chemically cross-linked, and proteins were denatured in 1% SDS for 30 min. SDS was diluted out to 0.1% by the addition of PBS before the addition of 20 μg of anti-HA (mAb 12CA5), rabbit anti-EXP2, or rabbit anti-HSP101 IgG (5) for 16 h at 4 °C. 100 μl of 50/50 slurry of protein G-Sepharose was to the lysate, and nonspecific proteins were removed by rinsing resin in 1% Triton X-100 before elution of bound proteins in 1× NRSB. Cross-links were reduced by the addition of 100 mM DTT (80 °C for 30 min). Samples were electrophoresed and Western-blotted.

Affinity Purification Assays with Differential Washing—Saponin-lysed 3D7 schizonts were solubilized in 10× pellet volume of 1% Triton X-100 with Complete protease inhibitors at room temperature for 6 h. Insoluble material was pelleted (14,000 rpm for 15 min), and 50 μg of either rabbit anti-EXP2 or anti-HA was added to the supernatant (16 h at 4 °C). 500 μl of protein G-Sepharose (1 h at 4 °C) was added to the lysate, and unbound material was removed by washing in 5 × 1 ml of either 1% Triton X-100, 0.5 radioimmune precipitation assay buffer (1% Triton X-100, 0.5% sodium deoxycholate, 0.05% SDS, 75 mM NaCl, 12.5 mM Tris-HCl, pH 8, in PBS) radioimmune precipitation assay buffer (1% Triton X-100, 1% sodium deoxycholate, 0.1% SDS, 150 mM NaCl, 25 mM Tris-HCl pH 8 in PBS), 500 mM NaCl in 1% Triton X-100, or 1 M NaCl in 1% Triton X-100. Bound proteins were eluted in 1× NRSB and analyzed by Western blotting. Bound antibody probes were as above, and densitometry of individual bands was calculated using ImageJ software.

Proteomic Analysis of PTEX and Cargo—150 ml of PTEX150-HA and HSP101-HA-mixed schizont and rings stages were grown and treated with tetanolysin (Sigma) as described previously (5) to permeabilize infected RBCs. After washing in PBS to remove the hemoglobin, immunoprecipitations were performed as specified for the pulse-chase analyses. After elution in 0.1 M glycine, pH 2.8, followed by 1× NRSB, samples were fractionated by SDS-PAGE in 4–12% bis-tris gels (Invitrogen). Gels were stained with GelCode Blue Safe Protein Stain (Pierce), and the protein constituents of excised bands were identified by LC/MS-MS at the Joint Proteomics Services Facility (Ludwig Institute for Cancer Research, Australia).

RESULTS

PTEX Components Reside in Merozoite Dense Granules and Subsequently in the PVM throughout the Ring Stage; the Time at Which PTEX Is Considered to Be Functional—Both PTEX150 and HSP101 have been localized previously to the apical region of merozoites, but the location of EXP2 at this cell cycle stage was unknown (5). We anticipated that EXP2 might be similarly located to the apical region as these three proteins are in a complex (5). Here we show by immunofluorescence microscopy that EXP2 does indeed co-localize with HSP101 at the merozoite apex (Fig. 1*A*).

To determine in which apical merozoite organelle the PTEX complex resides, immunofluorescence analyses of schizonts

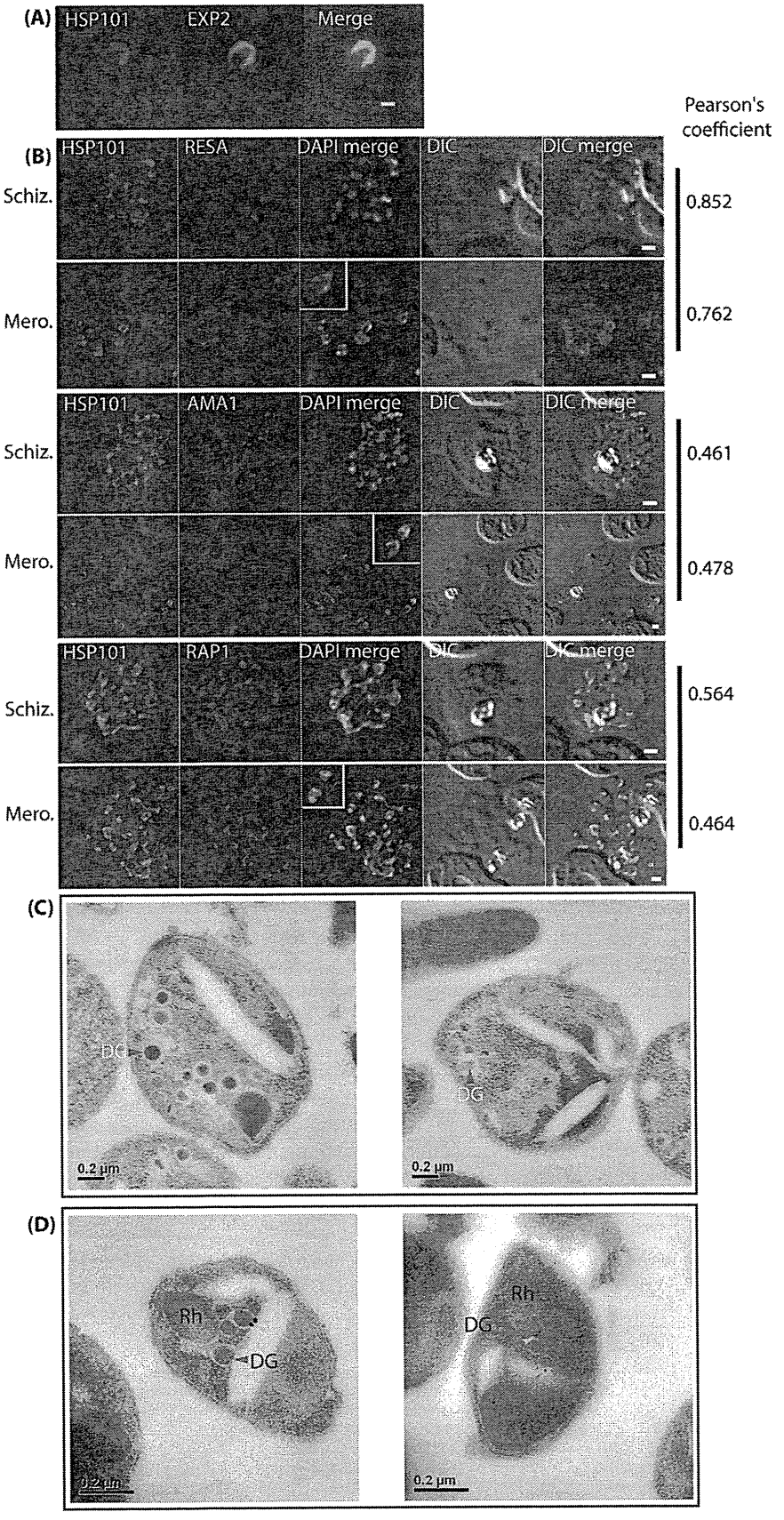

and merozoite stages were performed using rabbit anti-HSP101 antibodies in conjunction with mouse monoclonal antibodies to either the rhoptry-resident RAP1 protein, the microneme-resident AMA1 protein, or the dense-granule resident RESA protein (Fig. 1*B*). Because all three organelles form closely located punctate structures, it was difficult to definitively assign HSP101 to one of these compartments by eye (Fig. 1*B*). Pearson's coefficients were, therefore, measured for the images, with values close to one indicating a high degree of colocalization. The highest coefficients for HSP101 were found with RESA, indicating that the PTEX complex most likely resides within the dense granules.

To further validate these observations, immunoelectron microscopy was performed on merozoites purified from hemagglutinin-tagged PTEX150 (PTEX150-HA)-expressing parasites (Fig. 1, *C* and *D*). Cells were immunolabeled with anti-EXP2 or anti-HA antibodies. In both cases the immunogold label predominantly localized to small, round, electron dense vesicular structures of similar shape and size to that previously reported for dense granules (19) (Fig. 1, *C* and *D*). To exclude nonspecific labeling, anti-HA antibodies were used to label wild type parasites under the same conditions, and no labeled parasites were observed (supplemental Fig. 1).

The localization of PTEX components to the dense granules in merozoites suggested that PTEX is likely to be carried into the newly forming parasite and released into the developing PVM of ring stages. This was investigated through immunofluorescence assays of invading merozoites co-labeled for the tight junction marker RON4 (28) and PTEX components EXP2 and HSP101 (Fig. 2, *A* and *B*). During invasion, the tight junction is clearly visualized moving rearward along the parasite (RON4 label), whereas HSP101 and EXP2 labeling remains around the periphery of the parasite. This is consistent with localization to the dense granules that have been shown previously by immunoelectron microscopy to release their contents into the newly formed PV after invasion (21). Given that the remainder of the PTEX components (TRX2 and PTEX88) form a complex with HSP101, EXP2, and PTEX150, it is likely that these proteins also localize to the dense granules in merozoites and are thus similarly trafficked to the PV during invasion, but this remains to be formally demonstrated.

Examination of later ring stage parasites reveals that throughout these stages EXP2 and HSP101 continue to co-localize as distinct puncta in the PVM, indicative perhaps of distinct domains within this membrane (Fig. 2*C*). Previous immunoelectron microscopy of ring-stage parasites had indicated EXP2 resides at the PVM, occasionally to electron dense structures (7). In keeping with this, immunofluorescence analysis demonstrated HSP101 and PTEX150 do not co-localize with the parasite plasma membrane marker, MSP1 (5). However, given the extremely close apposition of the parasite plasma membrane and the PVM in ring-stage parasites, to definitively confirm the localization of PTEX at the PVM, we examined the location of EXP2 in schizont stages where the PVM is often more spatially separated from the plasma membrane of developing merozoites. For these experiments, sacks of unfiltered merozoites were prevented from bursting from their erythrocyte hosts by the protease inhibitor E64. These parasites were treated in an identical manner to the isolated merozoites in Figs. 1, *C* and *D*, with the exception that they were not filtered through a 1.2-μm filter before fixation. As can be seen in Fig. 2*D*, the anti-EXP2 antibody localized predominantly to the PVM, which is clearly distinguished from the plasma membranes of segmented merozoites. Somewhat unexpectedly, in these preparations the immunogold label preferentially labeled the PVM, whereas internal merozoite organelles, including dense granules, were predominantly unlabeled. This observation suggests that EXP2 accumulates to higher levels in the PVM than in the dense granules in schizont stage parasites, although this experiment is not quantitative, and we cannot exclude that the EXP2 antibody may preferentially access the PVM. Collectively, the above data suggest that the three major PTEX components reside in the merozoite dense granules and are released into the PV during invasion, where they then associate with the PVM.

Although Not All Co-expressed, PTEX Components Are Carried in to Newly Invaded Erythrocytes Where They Show Little Turnover during Ring Stages—Having demonstrated that PTEX proteins are present in merozoite dense granules and are carried into newly invaded erythrocytes (Figs. 1 and 2), we next explored when in the cell cycle these proteins are synthesized and whether after initial insertion into the PVM, the complex remains there for the duration of the cell cycle or if it is turned over. To investigate this, highly synchronized 3D7-PTEX150-HA and 3D7-HSP101-HA transgenic parasites were pulsed with [^{35}S]Met/Cys in cysteine/methionine-free media for 1 h at either schizont (38–42 h) or ring (4–8 h) stages. Samples were subsequently immunoprecipitated and analyzed by Western blotting to detect individual PTEX proteins and also through detection of the incorporated radiolabel to detect new material synthesized during the pulse period (Fig. 3). In samples pulsed during the schizont stage (Fig. 3*A*), incorporated radiolabel was detected for PTEX150 and HSP101, indicating that these proteins are translated during this time. However, EXP2 did not label under these conditions. Despite apparently not being synthesized during schizonts, substantial amounts of EXP2 are present at this life stage as indicated by Western blotting. After some loss during invasion, which is expected because this process is relatively inefficient *in vitro*, [^{35}S]Met/Cys-labeled PTEX150 and HSP101 then remained at

FIGURE 1. **PTEX components are apically localized in merozoite dense granules.** *A* and *B*, immunofluorescence assays were completed during schizogony and were probed for either PTEX components or markers of distinct organelles as indicated in each of the panels. *A*, merozoites probed with antibodies specific to both HSP101 and EXP2 demonstrate apical localization for both proteins. *B*, schizonts (*Schiz.*) and merozoites (*Mero.*) were labeled with antibodies specific to HSP101 and either RESA (dense granules), AMA1 (micronemes), or RAP1 (rhoptries). Co-localization quantitation reveals that HSP101 localizes most closely with dense granule associated RESA (*top two panels*) as indicated by the corresponding Pearson's coefficient (values closer to 1 represent greater co-localization). *Scale bar*, 1 μm. *DIC*, differential interference contrast. Immunoelectron microscopy of isolated D10 merozoites labeled with anti-EXP2 antibodies (*C*) and isolated PTEX150-HA merozoites labeled with anti-HA antibodies (*D*) indicate that immunogold labels (*yellow triangles*) localize to dense granules (*DG*) and not the rhoptries (*Rh*).

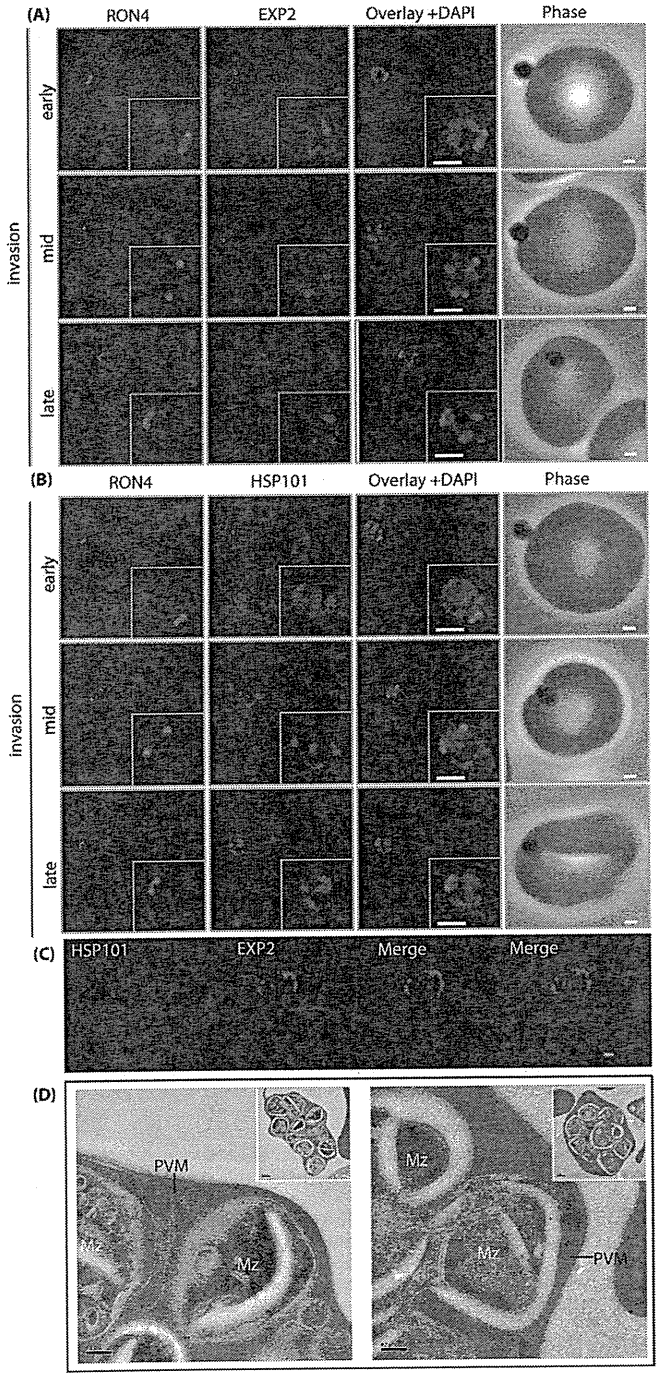

FIGURE 2. **PTEX components are carried into the newly infected erythrocyte and are present at the PVM throughout intraerythrocytic development.** *A* and *B*, shown is time-course of merozoite invasion by wide-field immunofluorescence microscopy with deconvolution (single slice shown) labeled for tight junction component RON4 and PTEX component EXP2 (*A*) or RON4 and PTEX component HSP101 (*B*). Both PTEX components are carried by the invading merozoite into the erythrocyte. *Scale bar*, 1 μm. *C*, HSP101 and EXP2 co-localize to distinct puncta at the PVM during later ring stage development. *Scale bar*, 1 μm. *D*, immuno-electron microscopy of unfiltered D10 merozoites within the erythrocyte clearly resolves the PVM from the merozoite (*Mz*) plasma membranes. High magnification of anti-EXP2 antibody labeling localized EXP2 to the PVM (with low magnification of the entire unfiltered cell provided in the *inset*), indicating that it is not a plasma membrane protein and that it remains on the PVM until the point of parasite egress from the erythrocyte.

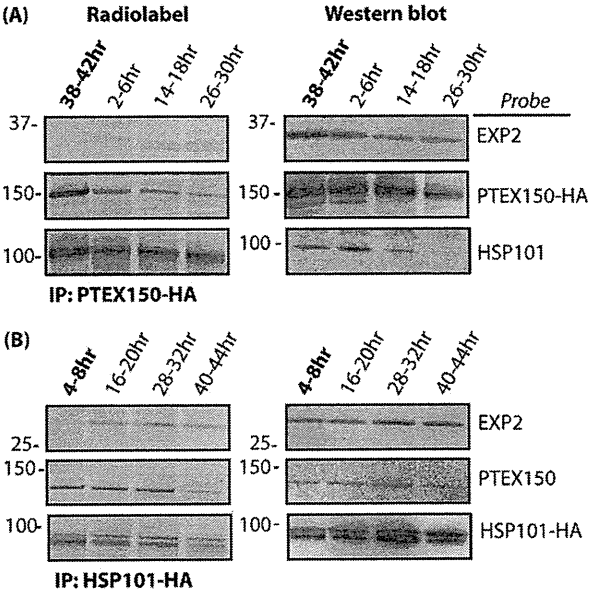

FIGURE 3. **Pulse-chase labeling reveals little protein turnover of PTEX components during the ring stages.** Schizonts (38–42 h) (*A*) or ring stage parasites (4–8 h) (*B*) were pulsed for 1 h with ^{35}S before chasing with unlabeled media for the remainder of the life cycle. Pulses were applied during the primary time point (*bold*) for each experiment. Material was immunoprecipitated (*IP*) using anti-HA to precipitate PTEX150-HA (*A*) or HSP101-HA (*B*) and their interacting partners. Eluted fractions were probed for the proteins indicated and radiolabel was detected by exposure to a PhosphorImager.

fairly constant levels until the last time point of the chase period, indicating that there is relatively little turnover of these proteins until the end of the ring stage (Fig. 3*A*, >24 h).

Samples pulsed in early rings also demonstrated radiolabel incorporation for PTEX150 and HSP101 (Fig. 3*B*), suggesting that biosynthesis of these proteins may continue throughout this period; however, it is difficult to rule out the possibility that low level schizont-merozoite contamination of the ring-stage preparation is responsible for this labeling. As was the case with the schizont-stage pulse, EXP2 was not radiolabeled during the early ring-stage pulse (Fig. 3*B*, *4–8 h lane*) but was effectively labeled at more mature ring stages (Fig. 3*B*, *16–20 h lane*), presumably due to the persistence of some ^{35}S[Met/Cys] in parasites during the chase period. Hence, although HSP101 and PTEX150 are synthesized majorly in schizonts and perhaps early rings, EXP2 is synthesized toward the middle of the erythrocytic cycle. These data for EXP2 are consistent with microarray analysis (22, 23) as well as recent time-course analysis of protein expression (24). Finally, it should be noted that for each of the three PTEX components examined here, there was no significant protein turnover during the ring-stage (0–24 h), suggesting that once the PTEX components appear at the PVM, they remain there for most of the 24-h ring stage and even beyond this time. Taken together, these analyses demonstrate that HSP101 and PTEX150 are synthesized before invasion as expected for proteins that reside in merozoite dense granules. Furthermore, although EXP2 is also present in merozoite dense granules, it is synthesized much earlier in the erythrocytic life cycle. The reason for this disconnect in the synthesis of proteins that ultimately co-localize is not yet understood.

PTEX Complex Is >1230 kDa and Contains ~600- and ~700-kDa EXP2 Homo-oligomers—For PTEX to carry out its putative role in translocating exported proteins across the PVM, it is assumed that its major constituent structural parts. HSP101, PTEX150. and EXP2, should assemble into a macromolecular complex. Given the putative role of EXP2 in forming a membrane-associated pore, it is expected that this protein may be present in a higher molecular weight homo-oligomeric species. Similarly, like other AAA^+ heat shock proteins, HSP101 is predicted to form a homo-oligomeric hexamer (5). Here we have investigated the oligomeric nature of each of these PTEX components via Blue Native PAGE (BN-PAGE) analyses.

For these analyses, parasite proteins were released from mixed stage parasite pellets through lysis with a variety of detergents including dodecylmaltoside, digitonin, CHAPS, β-octylglucoside, cell lytic buffer (40 mM Tris-HCl, pH 8.0, 1% propanesulfonate, and 0.1% 3-(4-Heptyl)phenyl-3-hydroxypropyl)dimethylammoniopropanesulfonate in PBS, pH 8.0) or Triton X-100. The resultant samples were analyzed by BN-PAGE and of the detergents tested Triton X-100 treatment alone demonstrated the most reproducible solubilization of PTEX components (data not shown) and was consequently used for all subsequent analyses. To determine the optimal conditions for resolution of PTEX-specific oligomers, a titration of Triton X-100 was employed (Fig. 4*A*). These analyses revealed that under lower concentrations of Triton X-100 (0.125, 0.25, and 0.5%) a >1230-kDa complex was detectable with EXP2-specific antibodies. Upon solubilization with 1% Triton X-100, however, two faster migrating fragments were released (~600–700 kDa; Fig. 4*A*, *left panel*). Under each Triton X-100 concentration tested, samples probed for HSP101 also displayed a single band detectable as >1230 kDa (Fig. 4*A*). However, no smaller HSP101 species were present under any condition tested.

Further analyses using the most disruptive of the conditions (1% Triton X-100) was pursued to further assess subfragments of the PTEX complex that may be released under these conditions (Figs. 4, *B* and *C*). Within the PTEX complex, HSP101 is proposed to form a hexameric ring, functioning as the ATPase to presumably facilitate protein translocation. It was, therefore, expected that this protein would form an ~600-kDa homo-oligomeric complex. Despite this, after repeated BN-PAGE analyses we were only able to detect HSP101 in a >1230-kDa species. The absence of smaller oligomeric or monomeric HSP101 species by BN-PAGE may suggest that HSP101 is more tightly bound to its direct interacting partner than EXP2 is and thus may not be released under the conditions tested here. Conversely, to detect HSP101 on BN-PAGE after transfer but before fixation of the proteins onto the membrane, membranes were treated with DTT and SDS. Only under these specific BN-PAGE conditions was HSP101 detectable. Such treatment may realistically cause less abundant HSP101 species to dissociate from the membrane before their fixation and subsequent detection, leaving behind the more prevalent >1230-kDa species.

Attempts were made to better resolve the EXP2-specific smear at ~600–700 kDa, including probing BN-PAGE blots with different EXP2-specific antibodies (mAb 7.7 and rabbit anti-EXP2). These analyses revealed the presence of EXP2 in three distinct bands at ~600, ~700, and >1230 kDa. The ~600- and ~700-kDa bands appeared to be specific and unique to EXP2 as they were detected by both rabbit and mouse monoclonal EXP2-specific antibodies (Fig. 4*C*). Furthermore, the two smaller EXP2-containing species did not label with antibodies recognizing the other major PTEX components HSP101 and PTEX150 (Fig. 4), suggesting that at least the smaller of these

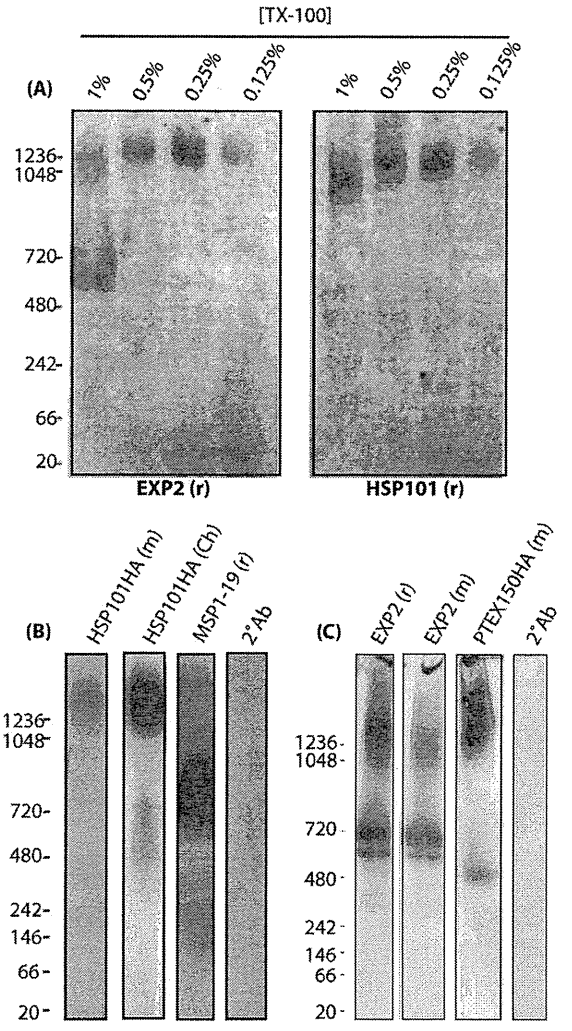

FIGURE 4. **BN-PAGE reveals that PTEX is a macromolecular complex of >1230 kDa that includes EXP2 oligomers of 600 and 700 kDa.** *A*, mixed stage parasites were solubilized with increasing concentrations of Triton X-100 as indicated *above the blots*. In 1% Triton X-100 (*TX-100*), EXP2 is present as a higher order oligomer (>1230 kDa) as well as a smaller species (~600–700 kDa). In lesser concentrations of detergent the smaller oligomeric species is not solubilized. In all conditions tested, HSP101 was only present in oligomeric species >1230 kDa. *B* and *C*, BN-PAGE analysis was completed for mixed-stage *P. falciparum* parasites solubilized with 1% Triton X-100, and resultant blots were probed for the indicated proteins. EXP2, PTEX150, and HSP101 are all present in large oligomeric complexes >1230 kDa. MSP1–19 was included as a control to ensure that the gels performed correctly and a specific ~600-kDa band could be detected as expected (27). *A* and *C*, EXP2 was additionally present in an homo-oligomeric species of ~600 and ~700 kDa. *B*, PTEX150 was present as an ~500-kDa homo-oligomeric species. *A* and *B*, HSP101 was solely detected in a band at >1230 kDa. *Control lanes* represent blots probed solely with secondary antibodies (*2°Ab*). *Letters in brackets* after proteins represent animal in which the antibody was raised. *m*, mouse; *r*, rabbit; *Ch*, chicken.

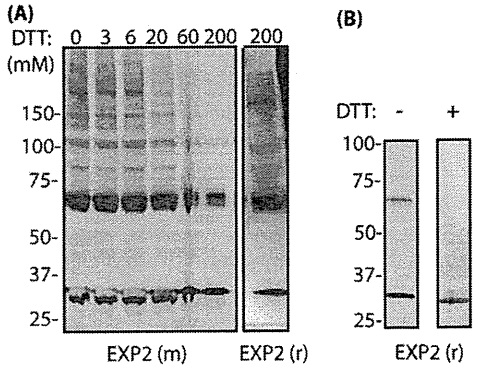

FIGURE 5. **EXP2 is present in higher order homo-oligomers.** Mixed-stage 3D7 parasites were cross-linked in 2 mM DSP and before electrophoresis were incubated in increasing concentrations of DTT to gradually break cross-links as indicated *above the blots*. Samples were Western-blotted and probed for the proteins indicated. *A*, EXP2 can be detected as a ladder of bands, the largest being an eight-mer. A doublet of bands is present at every second band in the ladder. *B*, when proteins were not cross-linked, the EXP2-specific dimer was present as a single band that collapsed down to a single monomeric species upon the addition of 100 mM DTT. *Letters in brackets after proteins* represent animals in which the antibody was raised. *m*, mouse; *r*, rabbit.

species may represent a homo-oligomer of EXP2 as discussed below.

PTEX150 was observed as a ~500-kDa species detectable by a PTEX150-specific antibody (Fig. 4*C*). Neither EXP2 nor HSP101 antibodies recognize this species, raising the possibility that it represents a homo-oligomeric form of PTEX150. As reagents are not yet available to the other known PTEX components, PTEX88 and TRX2, it is impossible to rule out their presence in either the EXP2 or PTEX150 subspecies. What is clear from this analysis is that the PTEX machine is a large complex of >1230 kDa and that stable 600- and 700-kDa subspecies of EXP2 are components of this complex.

EXP2 Displays Features of a Homo-oligomer Comprising at Least Eight Units—To examine the architecture of the EXP2 complexes, we used chemical cross-linking to stabilize protein-protein interactions before analysis by SDS-PAGE. Mixed blood-stage parasites were harvested and cross-linked with 2 mM concentrations of the reduction-sensitive, cell-permeable cross-linker dithiobis succinimidyl propionate. Before electrophoresis, cross-links were reduced by the addition of increasing concentrations of DTT (0, 3, 6, 20, 60, or 200 mM). This enabled the reduction of cross-links, releasing differentially sized oligomeric fragments detectable by Western blotting (Fig. 5). Probing of these samples with EXP2-specific antibodies revealed a ladder of bands separated by the approximate molecular mass of monomeric EXP2 with strong monomeric (~31 kDa) and dimeric (~62 kDa) subunits observed (Fig. 5). This ladder is consistent with EXP2 forming a large homo-oligomer. Under these conditions this ladder of bands could be resolved up to eight EXP2 subunits; however, less well resolved EXP2 species above this suggests that an EXP2 homo-oligomer comprises more than eight monomeric units. When probed for additional PTEX components HSP101 and PTEX150, no co-labeling bands were detected, indicating that these two components are not part of the detected EXP2 oligomer (data not shown).

Closer inspection of this EXP2-specific ladder revealed that every second species appears to be more strongly labeled, suggesting that a dimer is likely to form the core subunit of this EXP2-specific oligomeric species (Fig. 5). Furthermore, the cross-linked dimeric species appeared to migrate as a doublet, with the two species differing in size by 3–5 kDa. This doublet is not present in monomeric EXP2 (Fig. 5), indicating that it does not represent a post-translationally modified form of EXP2 or a cleavage product. This finding suggests that EXP2 may interact with an as yet unidentified polypeptide of 3–5 kDa that links dimeric units.

The nature of the dimeric EXP2 species was investigated further through use of non-cross-linked parasite samples prepared in non-reducing sample buffer. Samples were split into two fractions, and one-half was reduced (Fig. 5*B*). After Western blotting and probing with EXP2-specific antibodies, these analyses revealed the presence of an EXP2-specific dimer. This species appears to be reduction-sensitive as it collapses down into a single monomeric species upon addition of DTT (Fig. 5*B*).

EXP2 Is the Most Strongly Membrane-associated Component of the PTEX Complex—For the PTEX complex to function as a protein-exporting translocon, it must presumably contain a membrane-associated pore. Although membrane association of the PTEX components has been performed in the schizont stages (5), it has not been examined at the ring stages, i.e. the time at which the PTEX complex is presumably functioning. To investigate this, blood-stage parasites were harvested at the ring and schizont stages. After equinatoxin treatment to release soluble red cell proteins and hemoglobin, parasite proteins were extracted by initially freeze/thawing in PBS to release parasite soluble proteins and subsequently extracting the remaining proteins in a high pH carbonate buffer to separate peripheral membrane proteins from integral membrane proteins. Analysis of these fractions demonstrated that EXP2 consistently associates most strongly with the integral membrane-associated fraction both in schizont (as observed previously (5)) and ring-stage parasites (Fig. 6). The relative amounts of PTEX proteins in ring fractions as measured by densitometry are similar to schizonts (Fig. 6*B*) (5). This data suggest that of the three PTEX components analyzed here, EXP2 is the most likely to be directly membrane-associated in schizonts and rings, the time in which it presumably functions.

PTEX Complex Associates as EXP2-PTEX150-HSP101—To investigate the assembly of individual PTEX components and to provide evidence for direct protein-protein interactions between the major PTEX components, we performed two different co-immunoprecipitation approaches (Figs. 7 and 8). In the first approach, limiting amounts of the chemical cross-linker DSP were used to partially covalently link PTEX components. The assumption here is that directly interacting proteins would be more extensively cross-linked than would more distal proteins within the complex. Non-covalent protein-protein interactions were broken by high concentrations (1%) of the ionic detergent SDS followed by a 10-fold dilution of the detergent (0.1%) to enable antibody-mediated immunoprecipitations to be performed on this material. Individual proteins were detected by probing resultant Western blots for individual PTEX components (Fig. 7). Under the conditions used here, direct interactions were detected in samples where lesser amounts of cross-linker were used (0 and 0.5 mM), whereas

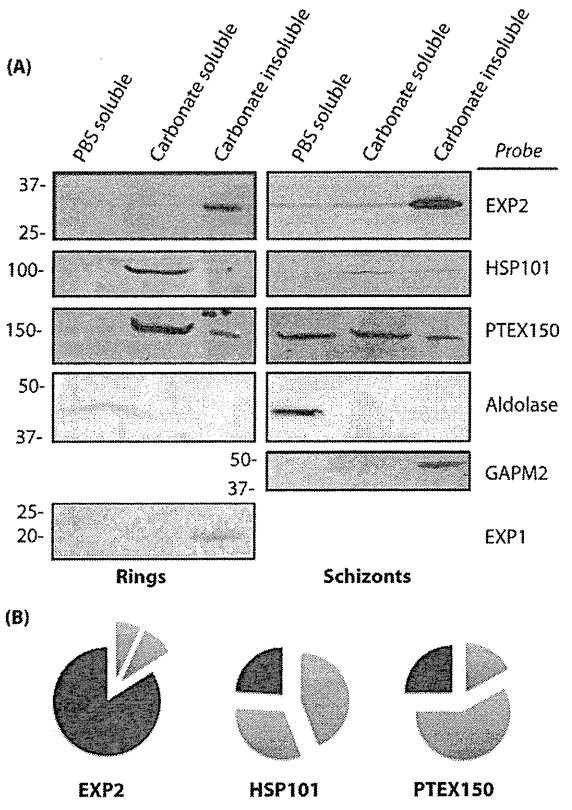

FIGURE 6. **EXP2 is the dominant membrane-associated PTEX component in both schizont and ring stages.** *A*, asexual blood stage *P. falciparum* parasites were extracted with PBS and sodium carbonate to separate soluble (PBS soluble), peripheral (carbonate soluble), or integral membrane proteins (carbonate pellet). Of the translocon components investigated, EXP2 is the most strongly associated with the integral membrane protein fraction in both rings and schizonts. The *bottom three panels* represent controls. Aldolase is a known soluble protein constitutively expressed throughout the intraerythrocytic lifecycle. GAPM2 is a schizont stage integral membrane protein. EXP1 is a ring stage integral membrane protein. *B*, densitometry was carried out on bands seen after carbonate extraction in ring stage parasites and was charted as the percentage of total material ($n = 2$ for each protein). *Blue*, PBS soluble. *Red*, peripheral membrane proteins. *Black*, integral membrane proteins.

indirect associations were detected after a greater level of protein cross-linking (1 and 2 mM). Densitometric analyses of subsequent Western blots revealed that HSP101 is most strongly cross-linked to PTEX150 but less so with EXP2 (Figs. 7, *A* and *B*), whereas EXP2 cross-linked more readily with PTEX150 but less so with HSP101 (Fig. 7*C*). This data suggests that these three major PTEX components are present in the order EXP2-PTEX150-HSP101.

To validate these results, an approach that does not rely on chemical cross-linking was employed and additional immunoprecipitation assays were performed in PBS with 1% Triton X-100. Once purified, the protein G-IgG-antigen complexes were washed using a range of detergent and salt conditions of increasing stringencies to assess for strength of interaction of the bound components. These wash buffers included (in order of increasing stringency) 1% Triton X-100, modified RIPA (1% Triton X-100, 0.5% sodium deoxycholate, 0.05% SDS, 75 mM NaCl, 12.5 mM Tris-HCl pH8 in PBS), RIPA (1% Triton X-100, 1% sodium deoxycholate, 0.1% SDS, 150 mM NaCl, 25 mM Tris-HCl, pH 8, in PBS), 500 mM NaCl in 1% Triton X-100, or 1 M NaCl in 1% Triton X-100. These wash steps were included to facilitate differentiation between tightly interacting proteins (those still present in co-immunoprecipitated fractions following washing in the more stringent buffers) from the peripherally associated proteins only detected when bound resin is washed in the least stringent buffers including 1% Triton X-100 and modified RIPA. After washing, bound proteins were eluted and analyzed by Western blotting (Fig. 8). To ensure that the stringent washes did not disrupt antibody binding to the primary antigen or between the antibody and protein G, the densitometry of the primary antigen was examined. In each case its density was much less reduced by the washes than the proposed interacting partners (Fig. 8). Taking this into consideration, HSP101 binds most strongly with PTEX150 (Fig. 8*A*), PTEX150 binds with similar strength to EXP2 and HSP101 (Fig. 8*B*), and EXP2 binds most strongly with PTEX150 (Fig. 8*C*). These data are consistent with cross-linking co-immunoprecipitation analyses presented in Fig. 7.

PTEX Comprises Stoichiometrically Similar Ratios of HSP101 and PTEX150 Bound to PEXEL Proteins—To approximate the ratios of PTEX proteins in the complex and possible PEXEL cargo proteins bound to PTEX, PTEX150-HA was immunoprecipitated from mixed schizont and ring stages and analyzed by mass spectrometry. To determine the constituents of specific co-immunoprecipitating protein bands, after fractionation by SDS-PAGE and staining with Coomassie, the lanes containing proteins from both eluted fractions were cut into 37 slices and assessed by LC/MS-MS (Fig. 9*A* and supplemental Fig. S2). From 5845 identified peptides (250 unique proteins), 825 (14%) were derived from the five known PTEX proteins, and 48 (1%) were from known or predicted PEXEL proteins (Fig. 9*B*). Most of the remaining proteins were low abundance contaminants probably not removed by the brief washing period. Many of the higher abundance non-PTEX/exported proteins *e.g.* dynamin (PF11_0465), CDC48 (PFF0940c), and COPI and COPII vesicular transport proteins, were detected in negative control immune precipitations of non-HA epitope-tagged 3D7 parasites performed previously by us (5) and probably bind to the IgG-agarose (indicated in supplemental Table S1).

Of the three exported proteins that co-precipitated with PTEX, PF08_0137 had the greatest number of peptides (41) (Fig. 9*B*). This protein belongs to the PHISTc family (3), and its interaction with PTEX was previously confirmed by high stringency immunoprecipitation experiments (5). Another protein previously shown to bind to PTEX was RESA (PFA0110w), and this was also observed here with four peptides (5). RESA contains a dnaJ domain, and interestingly so did the other exported protein that co-precipitated with PTEX-PFE0055c (three peptides).

In the PTEX150-HA immunoprecipitation we detected 385 peptides of this protein (2nd highest number) and remarkably a similar number of peptides from its direct binding partner HSP101 (392; highest number, Fig. 9*C*). Although mass spectrometry of peptides is only considered semi-quantitative of the actual protein levels, the high number of peptides and the similar size of PTEX150 and HSP101 suggests that these two proteins are probably in a similar stoichiometry in the PTEX complex. Therefore, if HSP101 forms a hexamer as is characteristic of the HSP100/ClpB family, then we predict there should be six

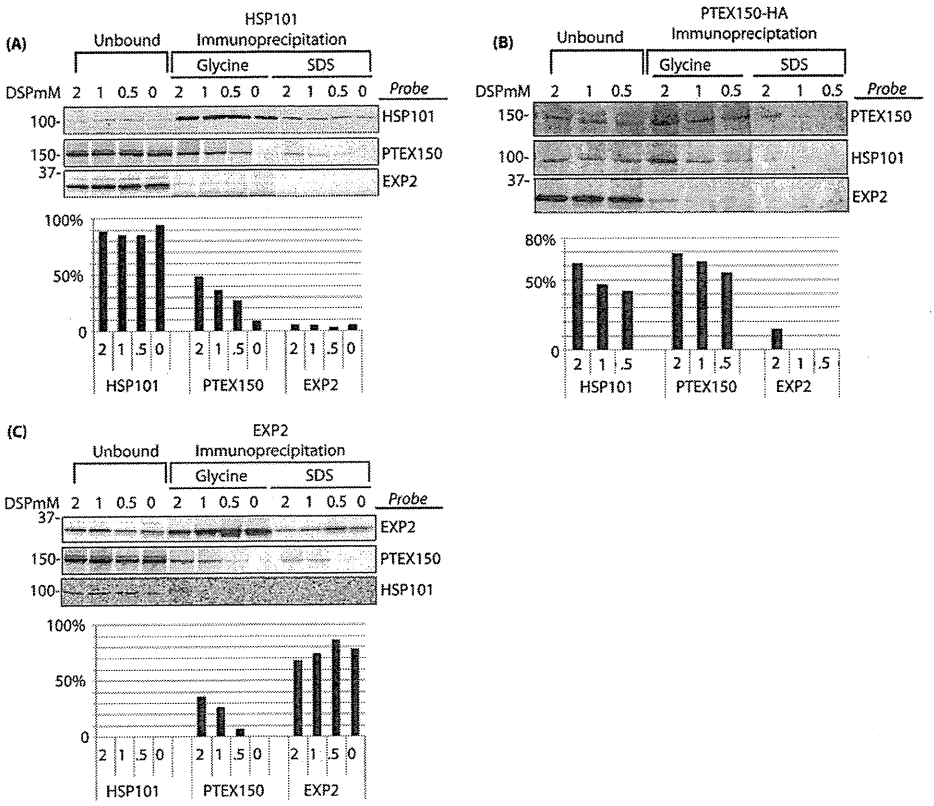

FIGURE 7. **Use of chemical cross-linking and differential reduction to identify direct protein-protein interactions within PTEX components.** Individual PTEX proteins were immunoprecipitated with either anti-HA antibodies directed to PTEX150-HA and HSP101-HA transgenic lines (*A* and *B*) or anti-EXP2 antibodies (*C*) as indicated at the *top of each panel*. Before immunoprecipitation, proteins were cross-linked with varying concentrations of DSP (mM) as indicated at the *top of each panel* and correspondingly on the *x* axis of each *bar graph*. Before electrophoresis, cross-links were broken by the addition of DTT. Stronger interactions are detected in lesser amounts of cross-linker. *A*, HSP101 demonstrated strongest binding to PTEX150. *B*, PTEX150 demonstrated stronger binding to HSP101 than EXP2. *C*, EXP2 demonstrated strongest binding with PTEX150. Percentage of bound protein is indicated for each immunoprecipitation beneath each series of Western blots.

PTEX150 molecules in the PTEX complex also. As anticipated, we detected the other three members of PTEX, namely EXP2, PTEX88, and TRX2 (15, 31, and 2 peptides, respectively; Fig. 9*C*). With proteins of differing sizes, percentage peptide coverage gives a better indication of abundance than peptide numbers alone. Unfortunately, the actual peptide sequences were not available, so we could not calculate total percentage coverage for the PTEX proteins. To obtain a measure of quantity, therefore, we have divided the number of peptides by protein length in amino acids, and here it is obvious that much more PTEX150 and HSP101 protein was precipitated than the other PTEX proteins (Fig. 9*C*). Nevertheless, a Coomassie-stained gel of the immunoprecipitation before excision of bands does suggest substantial amounts of PTEX88, EXP2, and TRX2 are present in these samples, and therefore, the proteomics analysis may have underestimated their quantities (Fig. 9*A*). One reason for the reduced yields of these proteins, particularly EXP2, is the prolonged overnight incubation of the parasite lysate in 1% Triton X-100 during the immunoprecipitation, which as we have demonstrated by BN-PAGE (Fig. 4) causes some EXP2 to dissociate from PTEX.

DISCUSSION

The *P. falciparum* translocon was originally identified as a complex of five different proteins including HSP101, EXP2, and TRX2 as well as the two hypothetical proteins, PTEX88 and PTEX150 (5). Here we have investigated the biosynthesis, localization, and macromolecular arrangement of three of these PTEX components: HSP101, PTEX150, and EXP2. In light of the data we have generated we put forward a new model for PTEX localization, biosynthesis, and interaction at the PVM (Fig. 10).

Previous studies of the PTEX complex have focused on the localization of its components in the ring stage, during which time the PTEX is likely to be functional. Image analyses completed here have confirmed this localization for EXP2. Additionally, immuno-electronmicroscopy confirmed that EXP2 and PTEX150-HA localize to the dense granules in extracellular parasites, and co-localization immunofluorescence analyses also demonstrated that HSP101 most closely co-localizes with the known dense granule marker and likely PTEX cargo protein RESA. Dense granules have been shown to secrete their contents into the forming parasitophorous vacuole during parasite invasion (25, 26), and localization to these organelles, therefore, implies that stored PTEX components are deposited directly into the PV membrane in which they are presumably functional. In support of this, we have shown that PTEX150 and HSP101 are synthesized mostly in schizonts and through into early rings, whereas peak EXP2 expression occurs late in the ring stage. There does not appear to be significant turnover of these proteins during the intraerythrocytic lifecycle, suggesting

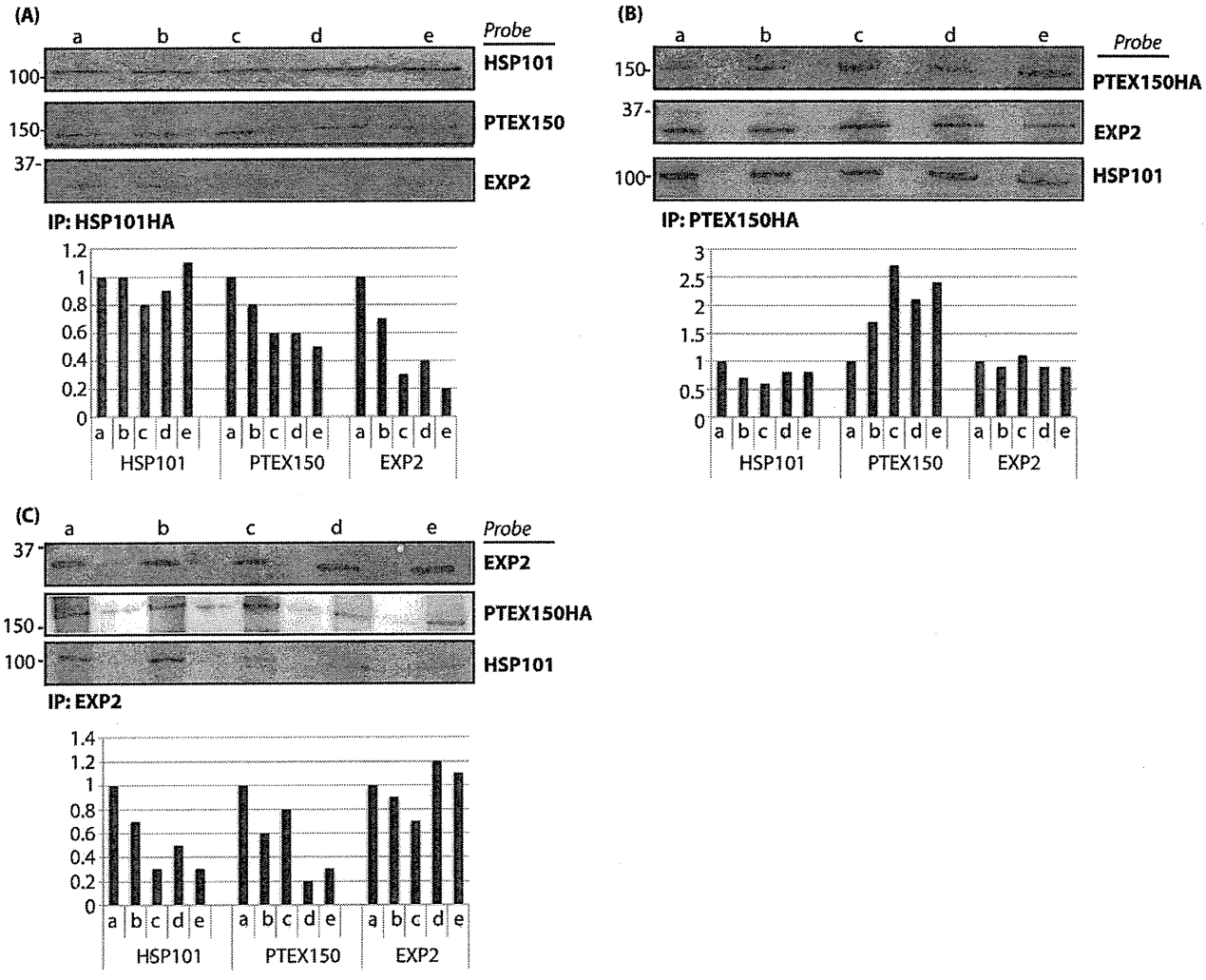

FIGURE 8. **An alternate approach to identify protein-protein interactions of PTEX components; PTEX susceptibility to increasing buffer stringency.** Individual PTEX proteins were immunoprecipitated from parasite lysates using either anti-HA antibodies to immunoprecipitate (*IP*) HSP101-HA and PTEX150-HA (*A* and *B*) or anti-EXP2 (*C*) antibodies as indicated. Buffers of varying stringency were used to wash off unbound proteins after immunoprecipitation as indicated at the *top of the panels* (increasing stringency from *left* to *right*). *A*, PTEX150 demonstrated equal binding for both HSP101 and EXP2. *B*, HSP101 showed stronger binding with PTEX150 than EXP2. *C*, EXP2 demonstrated a stronger association with PTEX150 than HSP101. Ratio of bound:unbound protein is represented by *bar graphs* beneath each immunoblot. Buffers included 1% Triton X-100 (*a*), 0.5 RIPA buffer (1% Triton X-100, 0.5% sodium deoxycholate, 0.05% SDS, 75 mM NaCl, 12.5 mM Tris-HCl, pH 8, in PBS) (*b*), RIPA buffer (*c*), 500 mM NaCl in 1% Triton X-100 (*d*), or 1 M NaCl in 1% Triton X-100 (*e*).

that once these proteins make it to the PVM, they reside there for the remainder of their functional lives. For EXP2 at least, this appears to be all the way through to merozoite egress. It should be noted that despite not being generated in schizonts, EXP2 protein is maximally detected by Western blotting and immunofluorescence assay (IFA) during these times, indicating that even though expression of these three PTEX components is not co-regulated, each is still present and co-located in both extracellular and intracellular stages. It remains to be determined as to why EXP2 is expressed much earlier than the other PTEX components.

Protein-translocating machineries are generally large oligomeric complexes associated with membranes where they function to enable the passage of proteins across membrane barriers. Until now, the macromolecular composition of the PTEX complex and the order in which each of its constituent parts assemble was unknown. Here we have demonstrated that HSP101, PTEX150, and EXP2 associate as EXP2-PTEX150-HSP101, with EXP2 associating most strongly with the PVM and thus being likely to serve as an anchor for the remainder of the PTEX complex. Furthermore, we have demonstrated that as expected, each of these components form high molecular weight oligomers detectable under BN-PAGE conditions. We have shown experimentally that the overall PTEX complex is >1230 kDa, which is within the predicted size range for this complex; HSP101 is expected to form a hexamer of 600 kDa, PTEX150 is expected to form an oligomer in stoichiometric ratio with HSP101 that would also generate an ~660-kDa oligomer, EXP2 potentially forms a 400-kDa 12-mer similar to HlyE, and finally at least one unit each of PTEX88 (90 kDa) and TRX2 (18 kDa) is expected to associate with this complex. Overall this would result in an estimated size of ~1800 kDa. Experimentally we have been able to detect an ~600-kDa EXP2-specific homo-oligomer as well as an ~500-kDa

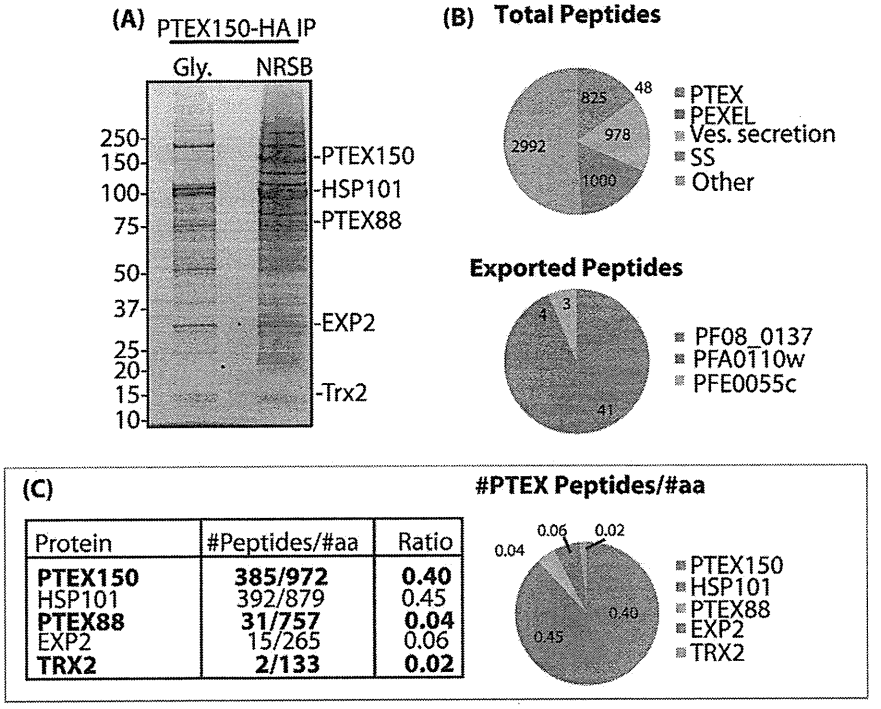

Protein	#Peptides/#aa	Ratio
PTEX150	**385/972**	**0.40**
HSP101	392/879	0.45
PTEX88	**31/757**	**0.04**
EXP2	15/265	0.06
TRX2	**2/133**	**0.02**

FIGURE 9. **Immunoprecipitation of PTEX150-HA followed by proteomic analysis indicates that PTEX150 and HSP101 are in similar ratios and probably bind to exported proteins.** *A*, PTEX150-HA and co-precipitating proteins were eluted in 0.1 M glycine, pH 2.8, followed by NRSB and were fractionated by SDS-PAGE in a 4–12% gradient gel. *B* and *C*, each lane was cut into 37 slices, and the co-migrating glycine and SDS slices were combined for subsequent LC/MS-MS to identify the proteins contained within. Pie charts of total peptide classes and exported proteins are shown. *C*, to establish the relative proportions of each PTEX protein in the complex, the numbers of peptides were divided by the number of amino acids in each of their sequences and represented in a pie chart.

PTEX150-specific homo-oligomer under BN-PAGE conditions. This PTEX150 oligomer is slightly smaller than expected; however, there is a 15% margin of error in predicting oligomer sizes using native-PAGE; therefore, the PTEX150 oligomer may realistically be in the range of ~425–575 kDa. Similarly, the detected size of the EXP2-oligomer is larger than that predicted for a 12-mer (400 kDa); however, if EXP2 indeed forms the putative membrane-associated PTEX pore, it would be expected to migrate slower by BN-PAGE when pore size is taken into consideration. Furthermore, EXP2 may form a pore much larger than a 12-mer given that it is presumably required to enable passage of unfolded proteins and not solely ions, as is the case for the HlyE pore. Whereas the exact protein content of this EXP2 oligomer is as yet unknown, we can conclude that HSP101 and PTEX150 are not components. Due to a lack of reagents to PTEX88 and TRX2, their absence or presence in either of these EXP2-specific bands is yet to be confirmed. It is unknown as to why EXP2 is consistently detected in two distinct oligomeric species; however, it is possible that the 700-kDa species represents a 600-kDa EXP2 oligomer bound up with an as yet unidentified interacting partner such as PTEX88 or multiple units of TRX2 or indeed a novel small molecular weight EXP2-interacting protein as suggested by chemical cross-linking experiments.

Chemically cross-linked EXP2 forms higher order oligomers resolvable to an 8-mer with what appears to be a core dimeric subunit apparent as a doublet of bands differing in size by ~5 kDa. This doublet is not present in monomeric EXP2 species, indicating that it is not likely to represent a degradation product. Furthermore, this doublet is only visible in every second band of the ladder, suggesting that each dimer is associated with a small putative protein. This putative EXP2 interacting protein may potentially play a role in assisting EXP2 dimerization or insertion of the putative EXP2 pore into the membrane and may explain the presence of two large oligomeric species during BN-PAGE. Conversely, this species may be an artifact of chemical cross-linking given that it is absent from non-cross-linked material. Further investigations via large scale immunoprecipitation and mass spectroscopic analyses of specific bands may reveal the true identity of this species.

Immunoprecipitation of PTEX150-HA followed by SDS-PAGE and proteomic analysis by LC/MS-MS indicates that these two proteins are tightly bound and apparently have a similar stoichiometry. Although PTEX150 migrates almost 50 kDa larger than HSP101, the two proteins have similar predicted molecular weights, indicating that peptide numbers are a good indicator of identical stoichiometry. At this stage we do not know if PTEX150 forms a hollow hexameric ring like that predicted for HSP101 or if it forms two or three 500-kDa dimers or trimers that link HSP101 to the EXP2 pore as suggested by our BN-PAGE analyses. Experiments presented here enabled us to identify three exported proteins co-purifying with PTEX, and because at least two of these interactions have been validated previously (5), we assume that all these exported proteins are putative cargos potentially en route through the PTEX complex. Not all exported proteins such as SBP1 and REX1 and -2 and the PfEMPs bear classic PEXEL motifs, and close inspection of the peptide list did not reveal the presence of these. This

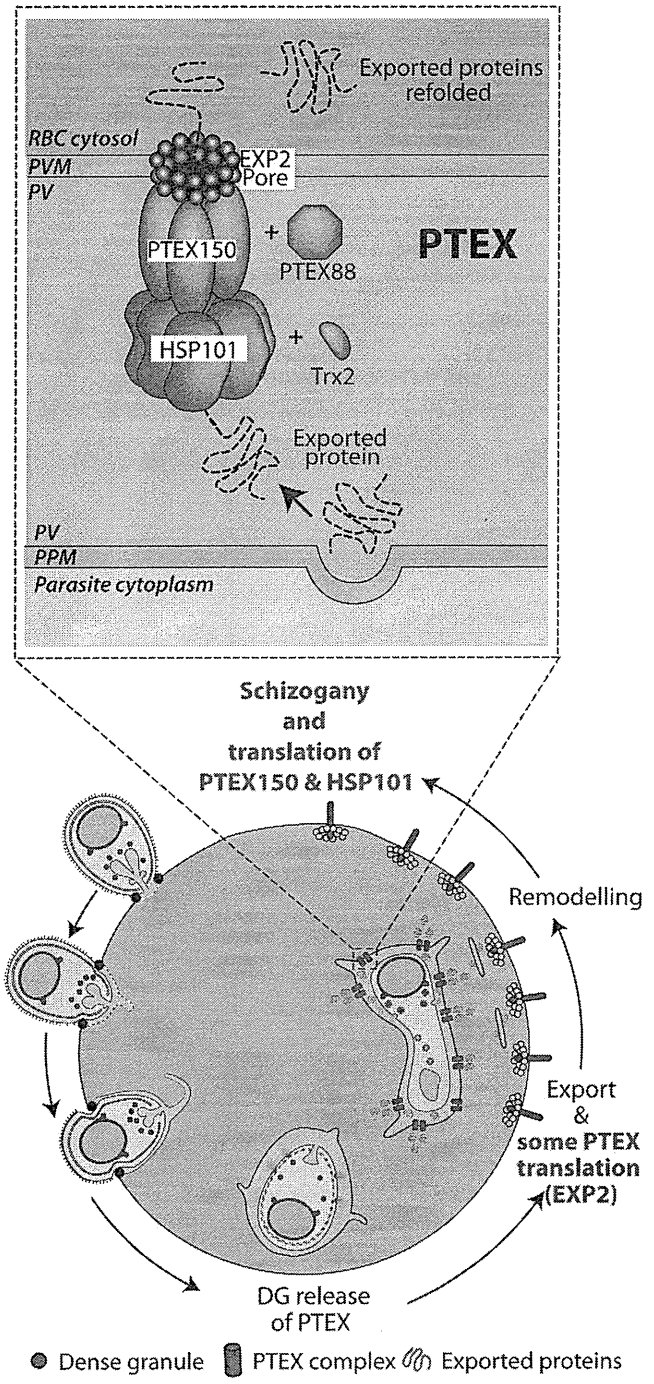

FIGURE 10. **A new model of PTEX interaction.** *Top panel,* shown is an expanded view of PTEX interaction at the PVM. EXP2 has demonstrated the strongest membrane association of the three major PTEX components (EXP2, HSP101, and PTEX150) and is believed to interact most strongly with PTEX150, which in turn binds HSP101. Data generated here indicate that the PTEX components PTEX150 and HSP101 are made predominantly in schizogony and are stored with EXP2 within the dense granules (*DG*) before their release into the newly forming PVM during invasion. EXP2 is synthesized predominantly in the ring/trophozoite stage, and some synthesis of PTEX150 and HSP101 is also likely to occur during this stage.

raises the possibility that PEXEL-negative exported proteins may use an alternative route to gain entry to the RBC compartment. Conversely, in the cell cycle stages used for this analysis there may have been a greater proportion of schizonts than actively exporting ring stages. This scenario is supported by the fact that the exported proteins we did identify have peak expression in schizonts as indicated by microarray data (22, 23). Identifying a wider range of exported proteins may require samples highly enriched in rings; however, previous attempts to purify PTEX from these stages resulted in samples heavily contaminated with RBC cytoskeletal proteins. To address this we may need to develop novel purification processes to ultimately reveal additional PTEX cargo.

Overall, these data demonstrate that PTEX components are synthesized before invasion and are stored in dense granules. Upon invasion these proteins are released into the newly formed PVM where they form a large, >1230-kDa complex consisting of detectable 600- and 700-kDa EXP2 homo-oligomers that are bound to a tightly linked complex of PTEX150 and HSP101. This PTEX150-HSP101 complex is itself >1230 kDa and comprises a similar stoichiometry of both proteins, probably comprising 6 units of each. The EXP2-specific oligomer is membrane-associated and is composed of dimeric subunits that presumably oligomerize to form the putative membrane-associated pore. Additionally, these data have revealed that there is no substantial turnover of the PTEX components deposited into the newly formed PVM, although we cannot rule out the synthesis of some functional PTEX machinery after invasion that traffics to the PVM via a different mechanism than dense granule release. Finally, these data are consistent with EXP2 forming a membrane-associated oligomer that serves to anchor the remainder of the PTEX components.

Acknowledgments—We thank the Australian Red Cross Blood Bank for the provision of human blood and serum, Jacobus Pharmaceuticals for providing WR99210, and the European Malaria Reagent Repository at the University of Edinburgh. We gratefully acknowledge the contribution to this work of the Victorian Operational Infrastructure Support Program.

REFERENCES

1. Hiller, N. L., Bhattacharjee, S., van Ooij, C., Liolios, K., Harrison, T., Lopez-Estraño, C., and Haldar, K. (2004) A host-targeting signal in virulence proteins reveals a secretome in malarial infection. *Science* **306,** 1934–1937
2. Marti, M., Good, R. T., Rug, M., Knuepfer, E., and Cowman, A. F. (2004) Targeting malaria virulence and remodeling proteins to the host erythrocyte. *Science* **306,** 1930–1933
3. Sargeant, T. J., Marti, M., Caler, E., Carlton, J. M., Simpson, K., Speed, T. P., and Cowman, A. F. (2006) Lineage-specific expansion of proteins exported to erythrocytes in malaria parasites. *Genome Biol.* **7,** R12
4. Goldberg, D. E., and Cowman, A. F. (2010) Moving in and renovating. Exporting proteins from *Plasmodium* into host erythrocytes. *Nat. Rev. Microbiol.* **8,** 617–621
5. de Koning-Ward, T. F., Gilson, P. R., Boddey, J. A., Rug, M., Smith, B. J., Papenfuss, A. T., Sanders, P. R., Lundie, R. J., Maier, A. G., Cowman, A. F., and Crabb, B. S. (2009) A newly discovered protein export machine in malaria parasites. *Nature* **459,** 945–949
6. El Bakkouri, M., Pow, A., Mulichak, A., Cheung, K. L., Artz, J. D., Amani, M., Fell, S., de Koning-Ward, T. F., Goodman, C. D., McFadden, G. I., Ortega, J., Hui, R., and Houry, W. A. (2010) The Clp chaperones and proteases of the human malaria parasite *Plasmodium falciparum*. *J. Mol. Biol.* **404,** 456–477
7. Johnson, D., Günther, K., Ansorge, I., Benting, J., Kent, A., Bannister, L., Ridley, R., and Lingelbach, K. (1994) Characterization of membrane proteins exported from *Plasmodium falciparum* into the host erythrocyte.

Parasitology **109,** 1–9
8. Mueller, M., Grauschopf, U., Maier, T., Glockshuber, R., and Ban, N. (2009) The structure of a cytolytic α-helical toxin pore reveals its assembly mechanism. *Nature* **459,** 726–730
9. Ludwig, A., Bauer, S., Benz, R., Bergmann, B., and Goebel, W. (1999) Analysis of the SlyA-controlled expression, subcellular localization, and pore-forming activity of a 34-kDa hemolysin (ClyA) from *Escherichia coli* K-12. *Mol. Microbiol.* **31,** 557–567
10. Eifler, N., Vetsch, M., Gregorini, M., Ringler, P., Chami, M., Philippsen, A., Fritz, A., Müller, S. A., Glockshuber, R., Engel, A., and Grauschopf, U. (2006) Cytotoxin ClyA from *Escherichia coli* assembles to a 13-meric pore independent of its redox-state. *EMBO J.* **25,** 2652–2661
11. Wallace, A. J., Stillman, T. J., Atkins, A., Jamieson, S. J., Bullough, P. A., Green, J., and Artymiuk, P. J. (2000) *E. coli* hemolysin E (HlyE, ClyA, SheA). X-ray crystal structure of the toxin and observation of membrane pores by electron microscopy. *Cell* **100,** 265–276
12. Trager, W., and Jensen, J. B. (1976) Human malaria parasites in continuous culture. *Science* **193,** 673–675
13. O'Donnell, R. A., de Koning-Ward, T. F., Burt, R. A., Bockarie, M., Reeder, J. C., Cowman, A. F., and Crabb, B. S. (2001) Antibodies against merozoite surface protein (MSP)-1(19) are a major component of the invasion-inhibitory response in individuals immune to malaria. *J. Exp. Med.* **193,** 1403–1412
14. Tsuboi, T., Takeo, S., Sawasaki, T., Torii, M., and Endo, Y. (2010) An efficient approach to the production of vaccines against the malaria parasite. *Methods Mol. Biol.* **607,** 73–83
15. Tsuboi, T., Takeo, S., Iriko, H., Jin, L., Tsuchimochi, M., Matsuda, S., Han, E. T., Otsuki, H., Kaneko, O., Sattabongkot, J., Udomsangpetch, R., Sawasaki, T., Torii, M., and Endo, Y. (2008) Wheat germ cell-free system-based production of malaria proteins for discovery of novel vaccine candidates. *Infect. Immun.* **76,** 1702–1708
16. Boyle, M. J., Wilson, D. W., Richards, J. S., Riglar, D. T., Tetteh, K. K., Conway, D. J., Ralph, S. A., Baum, J., and Beeson, J. G. (2010) Isolation of viable *Plasmodium falciparum* merozoites to define erythrocyte invasion events and advance vaccine and drug development. *Proc. Natl. Acad. Sci. U. S. A.* **107,** 14378–14383
17. Tonkin, C. J., van Dooren, G. G., Spurck, T. P., Struck, N. S., Good, R. T., Handman, E., Cowman, A. F., and McFadden, G. I. (2004) Localization of organellar proteins in *Plasmodium falciparum* using a novel set of transfection vectors and a new immunofluorescence fixation method. *Mol. Biochem. Parasitol.* **137,** 13–21
18. Bullen, H. E., Tonkin, C. J., O'Donnell, R. A., Tham, W. H., Papenfuss, A. T., Gould, S., Cowman, A. F., Crabb, B. S., and Gilson, P. R. (2009) A novel family of Apicomplexan glideosome-associated proteins with an inner membrane-anchoring role. *J. Biol. Chem.* **284,** 25353–25363
19. Bannister, L. H., Hopkins, J. M., Fowler, R. E., Krishna, S., and Mitchell, G. H. (2000) A brief illustrated guide to the ultrastructure of *Plasmodium falciparum* asexual blood stages. *Parasitol. Today* **16,** 427–433
20. Srinivasan, P., Beatty, W. L., Diouf, A., Herrera, R., Ambroggio, X., Moch, J. K., Tyler, J. S., Narum, D. L., Pierce, S. K., Boothroyd, J. C., Haynes, J. D., and Miller, L. H. (2011) Binding of *Plasmodium* merozoite proteins RON2 and AMA1 triggers commitment to invasion. *Proc. Natl. Acad. Sci. U. S. A.* **108,** 13275–13280
21. Torii, M., Adams, J. H., Miller, L. H., and Aikawa, M. (1989) Release of merozoite dense granules during erythrocyte invasion by *Plasmodium knowlesi*. *Infect. Immun.* **57,** 3230–3233
22. Bozdech, Z., Llinas, M., Pulliam, B. L., Wong, E. D., Zhu, J., and DeRisi, J. L. (2003) The transcriptome of the intraerythrocytic developmental cycle of *Plasmodium falciparum*. *PLoS Biol.* **1,** E5
23. Le Roch, K. G., Johnson, J. R., Florens, L., Zhou, Y., Santrosyan, A., Grainger, M., Yan, S. F., Williamson, K. C., Holder, A. A., Carucci, D. J., Yates, J. R., 3rd, and Winzeler, E. A. (2004) Global analysis of transcript and protein levels across the *Plasmodium falciparum* life cycle. *Genome Res.* **14,** 2308–2318
24. Foth, B. J., Zhang, N., Chaal, B. K., Sze, S. K., Preiser, P. R., and Bozdech, Z. (2011) Quantitative time-course profiling of parasite and host cell proteins in the human malaria parasite *Plasmodium falciparum*. *Mol. Cell Proteomics* 10.1074/mcp.M110.006411
25. Karsten, V., Qi, H., Beckers, C. J., Reddy, A., Dubremetz, J. F., Webster, P., and Joiner, K. A. (1998) The protozoan parasite *Toxoplasma gondii* targets proteins to dense granules and the vacuolar space using both conserved and unusual mechanisms. *J. Cell Biol.* **141,** 1323–1333
26. Trager, W., Rozario, C., Shio, H., Williams, J., and Perkins, M. E. (1992) Transfer of a dense granule protein of *Plasmodium falciparum* to the membrane of ring stages and isolation of dense granules. *Infect Immun.* **60,** 4656–4661
27. Sanders, P. R., Cantin, G. T., Greenbaum, D. C., Gilson, P. R., Nebl, T., Moritz, R. L., Yates, J. R., 3rd, Hodder, A. N., and Crabb, B. S. (2007) Identification of protein complexes in detergent-resistant membranes of *Plasmodium falciparum* schizonts. *Mol. Biochem. Parasitol.* **154,** 148–157
28. Richard, D., MacRild, C. A., Riglar, D. T., Chan, J. A., Foley, M., Baum, J., Ralph, S. A., Norton, R. S., and Cowman, A. F. (2010) Interaction between *Plasmodium falciparum* apical membrane antigen 1 and the rhoptry neck protein complex defines a key step in the erythrocyte invasion process of malaria parasites. *J. Biol. Chem.* **285,** 14815–14822

BAZF, a novel component of cullin3-based E3 ligase complex, mediates VEGFR and Notch cross-signaling in angiogenesis

*Hidetaka Ohnuki,[1-3] *Hirofumi Inoue,[1,3-5] Nobuaki Takemori,[6] Hironao Nakayama,[1,3] Tomohisa Sakaue,[4] Shinji Fukuda,[1] Daisuke Miwa,[1,7] Eiji Nishiwaki,[8] Masahiko Hatano,[9,10] Takeshi Tokuhisa,[9] Yaeta Endo,[2,11] Masato Nose,[12,13] and Shigeki Higashiyama[1,3,4]

[1]Department of Biochemistry and Molecular Genetics, Ehime University, Ehime, Japan; [2]Division of Cell-Free Science, Cell-Free Science and Technology Research Center, Ehime University, Ehime, Japan; [3]Strategic Young Researcher Overseas Visiting Program for Accelerating Brain Circulation, Japan Society for the Promotion of Science, Japan; [4]Department of Cell Growth and Tumor Regulation, [5]Ehime-NIKON Bioimaging Core-Laboratory, and [6]Proteomics Core-Laboratory, Protec Medicine Research Center (ProMRes), Ehime University, Ehime, Japan; [7]Fujirebio Inc, Tokyo, Japan; [8]Carna Biosciences Inc, Minatojima-Minamimachi, Kobe, Japan; [9]Department of Developmental Genetics, Graduate School of Medicine, Chiba University, Chiba, Japan; [10]Biomedical Research Center, Chiba University, Chiba, Japan; [11]Department of Medical Proteomics, ProMRes, Ehime University, Ehime, Japan; [12]Departmet of Pathogenomics, Ehime University Graduate School of Medicine, Ehime University, Ehime, Japan; and [13]Department of Immunopathology, ProMRes, Ehime University, Ehime, Japan

Angiogenic homeostasis is maintained by a balance between vascular endothelial growth factor (VEGF) and Notch signaling in endothelial cells (ECs). We screened for molecules that might mediate the coupling of VEGF signal transduction with down-regulation of Notch signaling, and identified *B-cell chronic lymphocytic leukemia/lymphoma6-associated zinc finger protein* (*BAZF*). BAZF was induced by VEGF-A in ECs to bind to the Notch signaling factor C-promoter binding factor 1 (CBF1), and to promote the degradation of CBF1 through polyubiquitination in a CBF1-cullin3 (CUL3) E3 ligase complex. *BAZF* disruption in vivo decreased endothelial tip cell number and filopodia protrusion, and markedly abrogated vascular plexus formation in the mouse retina, overlapping the retinal phenotype seen in response to Notch activation. Further, impaired angiogenesis and capillary remodeling were observed in skin-wounded *BAZF*$^{-/-}$ mice. We therefore propose that BAZF supports angiogenic sprouting via BAZF-CUL3-based polyubiquitination-dependent degradation of CBF1 to down-regulate Notch signaling. (*Blood.* 2012; 119(11):2688-2698)

Introduction

Vascular endothelial growth factor-A (VEGF-A) strongly stimulates endothelial cells (ECs) of preexisting blood vessels to break of their stable position in the vessel wall and jointly coordinate sprouting, branching, and new lumenized network formation. The tips of the sprouts are formed by specialized ECs called tip cells. Tip cells are migratory and extend numerous filopodia along gradients of VEGF-A. Following behind the tip cells, other ECs become stalk cells that proliferate and form the trunk of the new blood vessel.[1] Growing evidence during the past few years has established that the Notch signaling pathway plays a key role in coordinating multiple aspects of endothelial cell behavior in angiogenesis.[1] Recent genetic and pharmacologic studies in several systems demonstrate that the specification of ECs into tip and stalk cells is determined by a VEGF-Dll4/Notch cooperative negative or positive-feedback loop.[2-15] Interestingly, ECs in preexisting vessels express both Dll4 and Notch, and their signaling are thought to be balanced between adjacent ECs. VEGF stimulation somehow breaks this balance. Consequently Dll4 expression is up-regulated in presumptive tip cells, and induced Notch signaling in adjacent cells to become stalk cells.[16] However, the precise molecular mechanism to make such signal waves in adjacent cells is still unclear.

Recently, our studies of growth factors give a suggestive insight that a growth factor might signal not only to activate a growth promotion cascade, but also to unlock a growth suppression cascade via modulation of Zn-finger (ZnF)–type transcriptional repressors to progress cell growth coordinately.[17] A concept we felt might be applicable to the VEGF-Notch signaling in ECs at the tip cell position of angiogenic sprouts. Based on the idea, we also hypothesized that one or more of the numerous ZnF transcriptional repressors, most of whose functions still remain unknown, might be key players in this signaling.

To understand the "tug-of-war" balance between VEGFR and Notch signaling, it seems to be essential to perform more intimate analysis for VEGF-A–targeting genes. Therefore, we screened for molecules that are up-regulated in response to VEGF-A stimulation, and also impact on Notch signaling based on a C2H2-type ZnF cDNA micro array. Then, we intensively characterized the biochemical and biologic properties of candidate factors involved in the VEGFR-Notch cross signaling. These efforts resulted in the identification of *B-cell chronic lymphocytic leukemia/lymphoima6 (BCL6)–associated zinc finger protein* (*BAZF*) as a crucial factor in angiogenesis, linking the VEGFR and Notch signal transduction pathways by targeting C-promoter binding factor 1 (CBF1).

Submitted March 29, 2011; accepted December 26, 2011. Prepublished online as *Blood* First Edition paper, January 25, 2012; DOI 10.1182/blood-2011-03-345306.

*H.O. and H.I. contributed equally to this work.

The online version of this article contains a data supplement.

The publication costs of this article were defrayed in part by page charge payment. Therefore, and solely to indicate this fact, this article is hereby marked "advertisement" in accordance with 18 USC section 1734.

Methods

Constructs

cDNAs encoding BAZF, CBF1, and CUL3 were PCR-amplified and subcloned into the expression vector pME18S. Human *HEY1* promoter (3.9 kb)/pGL3 and Myc-N1ICD/pEFBOS were kindly provided by Drs Jiri Zavadil (NYU Langone Medical Center), Urban Lendahl (Karolinska Institute), and Tetsuya Taga (Tokyo Medical and Dental University), respectively.[18,19] Adenoviral vectors were constructed by Adenovirus Expression Vector Kit (Takara).

Cell culture and network formation

Human umbilical vein endothelial cells (HUVECs) were obtained from Cell Systems. HUVECs (6.5×10^3 cells/cm^2) were seeded onto solidified Matrigel (BD Biosciences). Before a treatment of 50 ng/mL VEGF-A (recombinant human VEGF165 protein; R&D systems), HUVEC were serum-starved for 12 hours. The images were analyzed by ImagePro Plus 4.5.1 (Media Cybernetics). In some experiments, DAPT (Calbiochem), cycloheximide (Wako), or MG132 (Sigma-Aldrich) were used as described in the figure legends. Time-lapse imaging analysis was performed using Eclipse TE300 microscope (Nikon) controlled by Simple PCI 6.60 software (Compix). HUVEC were infected with AdBAZF or control AdGFP at MOI of 50-250 and incubated for 18 to 24 hours before assays.

Microarray analysis

To identify VEGF-A response transcriptional regulators in HUVEC, 5 μg of total RNA was hybridized with a C2H2-type ZnF custom array (DNA Chip Research) and processed by CRBIOIIe/DNASIS Array ImageScanner (HitachiSoft) according to the manufacturer's protocol. All microarray data are available on the Gene Expression Omnibus (GEO) under accession number GSE35171.

Quantitative RT-PCR analysis

Total RNA (1 μg) was converted to cDNA using SuperScript III (Invitrogen) with oligo $(dT)_{20}$ primer. For real-time polymerase chain reaction (PCR) amplification, the primer sequences are listed in supplemental Table 1 (available on the *Blood* Web site; see the Supplemental Materials link at the top of the online article). Messenger RNA was quantified using SYBR green PCR master mix (Roche) or TaqMan gene expression assay by ABI Prism 7300 Fast Real-Time PCR system. The evaluation of relative differences of PCR product amounts among the treatment groups was carried out by the comparative cycle threshold method. The experiments were independently repeated at least 3 times, each performed in triplicate.

Gene silencing with small interfering RNA

HUVEC were transfected with small interfering RNA (siRNA) against human *BAZF* (15nM), *CBF1* (100nM), *Notch1* (100nM), or *CUL3* (100nM) by CodeBreaker (Promega) or RNAiMAX (Invitrogen) siRNA transfection regent. The siRNAs were purchased from Qiagen [human BAZF siRNA and control siRNA (1027098)] or Thermo Fisher Scientific [human CBF1 (L-007772-00), Notch1 (L-007771-00), and CUL3 (L-010224-00)]. Thirty-six hours after the transfection, HUVEC were serum-starved for 12 hours, and then treated with 50 ng/mL VEGF-A.

Immunoprecipitation and Western blotting

Immunoprecipitation was performed with anti-CBF1 (Abcam) or anti-FLAG (clone: M2, Sigma-Aldrich) antibody. The samples were subjected to sodium dodecyl sulfate polyacrylamide gel electrophoresis (SDS-PAGE), transferred to nitrocellulose membranes (Whatman) or Immun-Blot PVDF Membrane (Bio-Rad), and probed with an appropriate antibody. Antibodies are anti–human BAZF, biotinylated anti–human BAZF (Immuno-Biologic Laboratories), anti-CBF1, antiubiquitin (clone: P4D1, Cell Signaling Technology), anti-Notch1 (Abcam), anti–Cleaved Notch1 (Val 1744; Cell Signaling Technology), anti-FLAG, anti-V5 (R960-25, Invitrogen), anti-Myc (clone: 9E10, Calbiochem), anti–β-actin (clone: AC-15, Sigma-Ardrich), anti–β-tubulin (clone: JDR.3B8, Sigma-Aldrich), antilamin A/C (clone: 636, Santa Cruz), or anti-histone H3 (Upstate) antibody. The proteins were detected by ECL Plus Western Blotting Detection System (GE Healthcare). See supplemental Methods for further information.

HUVEC fibrin gel bead assay with adenovirus infection

HUVEC fibrin gel bead assay was carried out according to the method described by Nakatsu et al.[20] Briefly, 500 HUVEC were coated onto Cytodex-3 microcarrier (GE healthcare). HUVEC-coated beads were embedded in a fibrin clot in one well of a 12-well tissue culture plate. Human fibroblasts were plated on top of the clot. HUVEC were cultured for 3 days, and images were taken with an Olympus IX70 microscope (Olympus).

GST pull-down assay

GST, GST-CBF1, and GST-ZnF1-5 were prepared according to the protocol in the previous report.[21] The extracts from HT1080 cells expressing various V5-CBF1 or BAZF mutants were incubated with 5 μg of recombinant GST, GST-CBF1, or GST-ZnF1-5 immobilized on glutathione-Sepharose beads, and the bound proteins were analyzed by SDS-PAGE, followed by Western blotting using an anti-V5 antibody.

Luciferase assay

Human *HEY1* promoter (full-length, 3.9 kb)/pGL3 and Myc-N1ICD/pEFBOS were transfected with pRL-TK plasmid (Promega) into HUVECs. Twenty-four hours after transfection, the luciferase activities were measured using a dual-luciferase reporter assay system (Promega) according to the manufacturer's protocol.

Chromatin immunoprecipitation assay

A chromatin immunoprecipitation (ChIP) assay was performed according to the manufacturer's recommendation (Upstate) with the exception that the protein-DNA complex was precipitated by anti-CBF1 antibodies (Millipore) bound with Dynabeads-ProteinG (Invitrogen). The used primer sets are as follows: human HEY1 promoter, 5′-aattcagcggcgcgaga-3′ (forward) and 5′-ctcacgctttgcctctggtta-3′ (reverse); human *HEY2* promoter, 5′-cttgcggccgagcagagttg-3′ (forward) and 5′-gcttcatcccggcgaagacc-3′ (reverse). The precipitated genome DNA fragments were detected by ABI Prism 7300 Fast Real-Time PCR system with Power SYBR Green PCR Master Mix (Applied Biosystems).

Immunostaining

Immunostaining of HUVEC. HUVEC were fixed by 4% paraformaldehyde (PFA) and further treated with ice-cold methanol. Triton X-100–permiabilized cells were stained with anti-CBF1 (Abcam), anti-CUL3 (clone: 2236C1a, Bio-Matrix Research), anti-PML (clone: PG-M3, Santa Cruz Biotechnology), anti-SC35 (clone: SC-35, Sigma-Aldrich), and anti-Nucleolin (clone: 3G4B2, Upstate) antibodies. The nuclei were stained by Hoechst33342. Images were acquired by ImageXpress Micro (Molecular Devises), a confocal laser microscope A1 (Nikon) or a structured illumination microscope N-SIM (Nikon). Data were analyzed using MetaXpress (Molecular Devises) or NIS-Elements (Nikon).

Immunostaining of aortic frozen section. The cultured aortic pieces in type I collagen gel were sectioned by a cryostat and stained with an anti–mouse CD31 antibody (clone: MEC13.3, BioLegend) and Hoechst33342. Images were acquired by a confocal laser microscope Nikon A1.

Immunostaining of retina. Retinas for whole-mount immunostaining were fixed by 4% PFA overnight. Autoclaving process at 105°C for 15 minutes was performed as an antigen retrieval treatment of BAZF. After fixation, retinas were incubated in methanol at −30°C for 15 minutes. Retinas were stained with isolectin B4–Alexa Flour 647 in the presence or absence of anti-BAZF, anti-CBF1, or anti-HEY1 (Chemicon) antibodies.